Zhang *et al.*
Cell Communication and Signaling (2024) 22:456
https://doi.org/10.1186/s12964-024-01828-y

Cell Communication and Signaling

RESEARCH

Open Access

CXCR4 regulates macrophage M1 polarization by altering glycolysis to promote prostate fibrosis

Yi Zhang[1,2,3†], Chen Zhang[1,2,3†], Rui Feng[4†], Tong Meng[1,2,3], Wei Peng[1,2,3], Jian Song[1,2,3], Wenming Ma[1,2,3], Wenlong Xu[1,2,3], Xianguo Chen[1,2,3*], Jing Chen[1,2,3*] and Chaozhao Liang[1,2,3*]

Abstract

Background C-X-C receptor 4(CXCR4) is widely considered to be a highly conserved G protein-coupled receptor, widely involved in the pathophysiological processes in the human body, including fibrosis. However, its role in regulating macrophage-related inflammation in the fibrotic process of prostatitis has not been confirmed. Here, we aim to describe the role of CXCR4 in modulating macrophage M1 polarization through glycolysis in the development of prostatitis fibrosis.

Methods Use inducible experimental chronic prostatitis as a model of prostatic fibrosis. Reduce CXCR4 expression in immortalized bone marrow-derived macrophages using lentivirus. In the fibrotic mouse model, use adenovirus carrying CXCR4 agonists to detect the silencing of CXCR4 and assess the in vivo effects.

Results In this study, we demonstrated that reducing CXCR4 expression during LPS treatment of macrophages can alleviate M1 polarization. Silencing CXCR4 can inhibit glycolytic metabolism, enhance mitochondrial function, and promote macrophage transition from M1 to M2. Additionally, in vivo functional experiments using AAV carrying CXCR4 showed that blocking CXCR4 in experimental autoimmune prostatitis (EAP) can alleviate inflammation and experimental prostate fibrosis development. Mechanistically, CXCR4, a chemokine receptor, when silenced, weakens the PI3K/AKT/mTOR pathway as its downstream signal, reducing c-MYC expression. PFKFB3, a key enzyme involved in glucose metabolism, is a target gene of c-MYC, thus impacting macrophage polarization and glycolytic metabolism processes.

Keywords Macrophage, M1, Glycolysis, Chronic prostatitis, Fibrosis

†Yi zhang, Chen Zhang and Rui Feng contributed equally to this work.

*Correspondence:
Xianguo Chen
cxg7866186@126.com
Jing Chen
ayd_chenjing@163.com
Chaozhao Liang
liang_chaozhao@ahmu.edu.cn
[1] Department of Urology, the First Affiliated Hospital of Anhui Medical University, Anhui Medical University, Hefei, Anhui, People's Republic of China
[2] Institute of Urology, Anhui Medical University, Hefei, Anhui, People's Republic of China
[3] Anhui Province Key Laboratory of Urological and Andrological Diseases Research and Medical Transformation, Anhui Medical University, Hefei, Anhui, People's Republic of China
[4] Department of Urology, Shuguang Hospital, Shanghai University of Traditional Chinese Medicine, Shanghai 201203, China

Introduction

Chronic prostatitis is one of the most common diseases in adult males, with approximately 15% of men experiencing symptoms of prostatitis at some point in their lives [1]. The main symptoms during the course of the disease, apart from pain and lower urinary tract symptoms such as frequency, urgency, interruption of urination, and waiting to urinate, also seriously affect the quality of life of men. In the past, it was often thought to be secondary to inflammation of the prostate, increased volume, and the resulting increase in bladder outlet resistance or urethral sphincter contraction to explain. However, clinically, patients with prostatitis may experience LUTS even when their prostate volume is normal or slightly enlarged [2]. Prostate tissue specimens from patients with lower urinary tract symptoms(LUTS) commonly show inflammatory infiltrates, including T cells, B cells, macrophages, and so on [3]. Research has shown that prostatitis is related to prostate volume, and patients with chronic inflammation cell infiltration have a larger prostate volume compared to those without evidence of inflammation [4]. The severity of LUTS is also positively correlated with the degree of inflammation [5]. In epidemiological research, there is an association between chronic prostatitis and the subsequent occurrence of LUTS [6, 7]. Fibrosis occurs downstream of inflammation in terms of the mechanism [8], Chronic inflammation can cause damage to tissue cells, triggering abnormal healing responses, ultimately leading to fibrosis [9, 10]. Prostate fibrosis is characterized by the accumulation of myofibroblasts, collagen deposition, extracellular matrix (ECM) remodeling, and increased tissue hardness [3, 8, 11]. Prostate fibrosis occurs under the stimulation of inflammation, leading to organ stiffness, disappearance of normal tissue structure, and thus adversely affecting lower urinary tract function, resulting in changes in voiding symptoms.

In young men, only a small number of immune cells infiltrate the prostate gland. When inflammation occurs, a large number of immune cells, mainly including T cells and macrophages, will infiltrate [12]. Macrophages recruited in particular in prostatitis have been identified as key regulatory factors in prostatitis. In clinical practice, phospholipid vesicles are often used as an indicator to some extent to assess the severity of chronic prostatitis. Due to the decrease of phospholipid vesicles and the phenomenon of clustering during the inflammatory process, it indicates that the macrophages in the area of inflammation engulf a large amount of lipids. Research has also pointed out that macrophages infiltrated in nerve tissues, especially in the nerve ganglia near the prostate, may be one of the causes of autoimmune prostatitis pain [13]. Macrophages have been widely studied for their impact on fibrosis in various diseases. [14, 15], renal [16], liver [17], lung [18] etc. In fact, fibroblasts and macrophages are present in all organs, usually closely connected to each other and may regulate each other as a feedback loop [19]. However, research on macrophages in prostate fibrosis has not been extensively studied.

CXCR4 is a chemokine receptor that plays a regulatory role in many diseases and is essential during embryonic development. CXCR4 knockout mice exhibit embryonic lethality, with defects in vascular development, hematopoiesis, and heart formation [20]. The CXCL12/CXCR4 pathway promotes the involvement of inflammatory cells in the occurrence and development of inflammatory reactions. At the same time, CXCL12/CXCR4 promotes the recruitment of key effector cells such as myofibroblasts and macrophages to the site of tissue damage [9]. The role of CXCR4 in inflammation has been widely studied over the past thirty years. However, CXCR4 is widely considered to be a pro-fibrotic protein, but previous research has mainly focused on its pro-fibrotic function in mesenchymal cells such as myofibroblasts, rather than its pro-fibrotic function in inflammatory cells such as macrophages [21, 22]. PFKFB3 plays an important regulatory role in the energy metabolism of glycolysis, and fructose-2,6-bisphosphate is the most potent allosteric activator of phosphofructokinase-1, which can function within physiological concentrations. Its driven glycolysis plays a crucial role in endothelial cells and myeloid cells [23, 24].

Activation of CXCR4 can regulate multiple downstream signaling pathways, with the PI3K/AKT pathway being particularly important. Signaling through the phosphoinositide 3-kinase pathway promotes the activation of downstream effects and cell polarization, which is the first step in cell migration [25]. The PI3K/AKT pathway not only transmits metabolic information, but also regulates changes within macrophages, leading them to shift towards a more pro-inflammatory state [26]. Previous studies have shown that the PI3K/AKT pathway plays a crucial role in guiding the interaction between macrophages and adipocytes, and this mechanism is considered to be the basis of metabolic inflammatory responses [27]. Notably, previous studies have highlighted the important upstream role of the PI3K/AKT pathway in chronic prostatitis inflammation [28–30]. However, it is still unclear whether the activation of the PI3K/AKT pathway in macrophages plays a role in regulating the fibrotic process of chronic prostatitis.

Increased infiltration of prostate macrophages has been observed in patients with chronic prostatitis/chronic pelvic pain syndrome (CP/CPPS) as well as in EAP mice. This heightened macrophage presence is closely associated with the worsening of the disease and

the intensification of pain symptoms [31, 32]. Deletion of GM-CSF in EAP mice has been shown to significantly alleviate pain symptoms, suggesting a critical role for GM-CSF in the modulation of pain in this model [33]. Macrophages, which serve as a key marker of inflammatory infiltrating cells in prostatitis, can be categorized into various functional subtypes. These include the classically activated M1 type, the alternatively activated M2 type, and other phenotypic variations, each playing distinct roles in the inflammatory response and disease progression [34]. M1 macrophages are widely recognized for their role in promoting inflammatory responses through the secretion of substantial amounts of inflammatory cytokines. However, the intrinsic properties of macrophages, their various subtypes, and their connection to organ fibrosis remain incompletely understood. Further research is needed to elucidate these relationships and their implications for disease progression and treatment [28, 35, 36]. In particular, gaining a deeper understanding of the roles of macrophages, as well as the interaction dynamics and molecular mechanisms between macrophages and fibroblasts, could pave the way for the development of novel, personalized therapeutic strategies aimed at preventing or alleviating the progression of EAP.Here, we aim to describe the role and mechanism of macrophage CXCR4 in prostatic fibrosis. We found that CXCR4 drives macrophage glycolytic metabolism by affecting PFKFB3 transcriptional regulation. Furthermore, we observed that in vivo inhibition of CXCR4 expression reduces inflammation and macrophage M1 polarization infiltration in a mouse model of chronic prostatitis. Finally, we discovered that CXCR4-silenced macrophages can affect fibroblast fibrosis, revealing the relationship between M1 macrophages and prostatic fibrosis. Therefore, we have uncovered the central role of CXCR4 in macrophage metabolism and in maintaining fibrosis in chronic prostatitis.

Materials and methods

Cell lines, treatment and knockout

Cultivate the immortalized bone marrow-derived macrophage cell line iBMDM, embryonic fibroblast cell line(3T3), and HEK293T cells in high-glucose DMEM medium supplemented with 10% fetal bovine serum (FBS) (Cat# BC-SE-FBS07, Biochannel) and 1% penicillin–streptomycin (Cat# C0222, beyotime). The iBMDM macrophages were gifted by Professor Feng Shao. To begin, evenly distribute 2×10^6 cells per well in a six-well plate. The following day, replace the cell supernatant with 1 ml of fresh medium, then add the virus at a multiplicity of infection (MOI) of 25 (virus titer: 2×10^8 TU/ml) and polybrene at 8 μg/ml. Incubate in the cell culture incubator for 24 h. After incubation, discard the supernatant, and add puromycin dihydrochloride (5 μg/ml) to select for successfully transfected cells. To induce macrophage polarization, treat the cells with LPS (100 ng/ml) (Cat# HY-D1056, MCE) for 24 h. For the knockdown of CXCR4 in macrophages, transfect iBMDM cells with a lentiviral vector containing CXCR4-targeting sequences. The oligonucleotide sequences specifically targeting CXCR4 and Pfkfb3 were as follows: Sh CXCR4: TGTTTCAATTCCAGCATATAA, Sh Control: TTCTCCGAACGTGTCACGTAA, si NC: UUCUCC GAACGUGUCACGU, si CXCR4: GGUUACCAGAAG AAGCUAA, si Pfkfb3: GAUAGGUGUUCCAACGAAA. For transient transfection procedures, use Lipofectamine 3000 (Invitrogen, Thermo Fisher Scientific) to transfect plasmids and siRNA into the cells.

After cutting open the tibia and femur of the mouse, rinse the bone marrow cavity with cold PBS to extract bone marrow mononuclear cells. Treat the extracted cells with ACK lysis buffer for 15 min to lyse red blood cells, then wash the cells once with PBS. Culture the cells in RPMI-1640 medium supplemented with 10% fetal bovine serum and 25 ng/ml Macrophage Colony-Stimulating Factor (M-CSF) for one week. On the fourth day, replace the culture medium with fresh medium. The adherent cells remaining after this process will be used for subsequent experiments. Incubate the cells at 37 °C with 5% CO2. All cell lines used in experimental research have a passage number of less than twenty.

Patient samples

All clinical prostatic samples were obtained from the First Affiliated Hospital of Anhui Medical University (Anhui, China, Approval No: PJ2024-04–30), consisting of 26 paraffin-embedded prostate tissue slices. Analysis of all specimens by patients was obtained with informed consent. All human studies were conducted with the approval of the Medical Ethics Committee of Anhui Medical University.

Construction of a mouse model of EAP and evaluation of pelvic pain symptoms

For the construction of experimental autoimmune prostatitis (EAP), NOD male mice were obtained from the Nanjing Biomedical Research Institute at Nanjing University. All in vivo experimental protocols were authorized by the Animal Center of Anhui Medical University (Approval No: LLSC20211051). Prostate tissues from SD rats were ground to obtain prostate antigens, which were then emulsified in equal amounts of complete Freund's adjuvant to prepare the immunizing reagent. Subsequently, on day 0 and day 28, 300 μg of the immunizing reagent was injected subcutaneously at various sites such as the base of the tail and hind paws of male NOD mice.

The mouse modeling was divided into two phases. In the first phase, the EAP mice were divided into two groups, with one group receiving intraperitoneal injections of AMD3100 (5 mg/kg/d, soluble in PBS) (Cat# GC14745, glpbio) and the control group receiving an equal amount of PBS via intraperitoneal injection for 14 consecutive days. After sacrificing these two groups of mice, the prostate tissues were collected for transcriptome sequencing and untargeted metabolome sequencing. In the second phase, EAP mice with reduced CXCR4 expression using adenovirus-associated vectors were constructed. Mice injected with Sh NC-AAV via the tail vein served as the control group. In the third phase, following the establishment of the EAP model, 3PO, a PFKFB3 inhibitor, was administered via intraperitoneal injection at a dosage of 30 mg/kg every other day for three weeks. All mice injected with adenovirus-associated vectors were first injected with 100 μl of virus via the tail vein, followed by two subcutaneous immunizations for the construction of EAP model two weeks later. After 14 days of model construction, the reaction frequency of various fibers in the pelvic stimulation of mice in each group was tested before euthanasia. A positive pain response was considered if one of the following three reactions occurred: (a) severe abdominal contractions, (b) immediate scratching or licking of the area stimulated by the fibers, or (c) jumping.

Hematoxylin–Eosin (HE) staining

After dehydration, the paraffin sections are first stained with hematoxylin for 5 min, followed by rinsing with water. The sections are then treated with a differentiation solution, rinsed again, and subsequently incubated and rinsed before proceeding to eosin staining. The slides are dehydrated in 95% ethanol for 1 min, treated with eosin solution for 15 s, and finally mounted with neutral resin. The severity of inflammation is classified into four levels: 0 = no inflammation, 1 = mild inflammation with evident mononuclear cell infiltration around blood vessels, 2 = moderate mononuclear cell infiltration around blood vessels, 3 = vessels significantly curved, bleeding, and rich mononuclear cell infiltration.

Immunohistochemistry (IHC) assay

The paraffin-embedded tissue sections were deparaffinized and subjected to antigen retrieval, followed by three washes. The sections were then immersed in a 3% hydrogen peroxide solution and incubated in the dark at room temperature for 25 min to block endogenous peroxidase activity. After blocking with 3% BSA serum, the primary antibody was applied at an appropriate dilution and incubated overnight at 4 °C. Following this, the sections were washed three times with wash buffer. The sections were then incubated with the corresponding HRP-labeled secondary antibody at room temperature for 60 min. After washing, the sections were dried and treated with DAB chromogenic solution. The reaction was stopped by rinsing the sections under running water. Counterstaining was performed with hematoxylin to stain the cell nuclei. Finally, the sections were dehydrated, sealed, and observed under a microscope.All primary antibodies are listed in Table S1.

Immunofluorescence

After dewaxing the paraffin sections, antigen retrieval is performed using EDTA buffer (pH 6.00), followed by three washes to remove excess liquid and block antigens. The sections are then incubated overnight at 4 °C with the primary antibody prepared at a specific dilution. Following this, the appropriate secondary antibody is applied and incubated at room temperature in the dark for 2 h. For nuclear staining, the sections are treated with DAPI dye and incubated in the dark at room temperature for 10 min. Finally, the sections are sealed with a fluorescence quenching reagent, and evaluation and imaging are performed using a fluorescence microscope. All primary antibody information is listed in Table S1.

Masson staining

The Masson staining kit was purchased from Servicebio (Cat# G1006). Following dewaxing paraffin sections and rehydration to water, immerse the sections in Masson A solution overnight, rinse with tap water. Then immerse the sections in a mixture of Masson B solution and Masson C solution at a 1:1 ratio for 1 min, rinse with tap water, differentiate in differentiation solution for several seconds, rinse with tap water. Immerse the sections in Masson D solution for 6 min, followed by immersion in Masson E solution for 1 min. Without rinsing, remove excess liquid and directly immerse the section in Masson F solution for 20 s. Finally, rinse the sections with 1% acetic acid for differentiation, dehydrate with ethanol, and mount with a coverslip.

Sirius red staining

The Sirius Red staining solution was obtained from Servicebio (Cat# G1018). Begin by Dewax the paraffin sections and rehydrating them to water, stain with Sirius Red staining solution: stain the sections in Sirius Red staining solution for 8 min, dehydrate in absolute ethanol; mount coverslips after dehydration.

RNA isolation and RT-qPCR

According to the reagent kit instructions, use ESscience RNA-quick purification technology to separate RNA from total prostate tissue (Cat# RN002plus; YiShan

Biotech) and cells (Cat# ES-RN001; YiShan Biotech). Then, measure the purity and concentration of RNA using a NanoDrop 2000 spectrophotometer. Reverse transcription is performed using the PrimeScript™ RT kit, and qPCR reactions are prepared using SYBR Green Mix, with a final volume of 20μL. All primers are synthesized by General Biology. The primer sequences used are listed in Table S2. To elucidate the relative gene expression levels, the $2^{-\Delta\Delta CT}$ method is employed, with β-actin as the internal reference for data normalization.

Western Blotting (WB)

Use RIPA lysis buffer (Beyotime), supplemented with PMSF and a complete mixture of phosphatase and protease inhibitors, to extract total cellular proteins. The proteins are then separated by 12.5% SDS-PAGE gel electrophoresis and transferred to a NC membrane (Bio-Rad, Hercules). Block the membrane with 5% non-fat milk at room temperature for 1 h, then incubate with the primary antibody overnight at 4 °C. After washing, incubate with the secondary antibody for 2 h. β-actin is used as an internal reference for normalizing total protein levels.

Co-culture

First, polarize the macrophages transfected with Sh NC and Sh CXCR4 by inducing with LPS (100 ng/ml) for 24 h. The following day, discard the supernatant and gently tap the cells to detach them, then wash the cells three times with PBS. Plate the 3T3 cells in the bottom layer of a six-well co-culture plate (Cat# 3412, Corning), and place the macrophages in the co-culture chamber. Continue to culture for an additional 24 h, then collect the 3T3 cells for the corresponding experimental tests.

RNA-seq

Following the the kit instructions, total RNA was extracted using TRIzol reagent. The quantity and purity of the RNA were assessed using a NanoDrop 2000 spectrophotometer, while RNA integrity was evaluated using the Agilent 2100 Bioanalyzer. The construction of the transcriptome library was performed using the VAHTS Universal V5 RNA-seq Library Prep Kit. The library was sequenced on the Illumina Novaseq 6000 platform. For differential gene expression analysis, the DESeq2 package was used, and genes with a q-value < 0.05 and $|logfc| > 1$ were defined as differentially expressed genes (DEGs).

Non- targeted metabolomics

Place 20 mg of prostate tissue into a 1.5 mL EP tube, add 2 small steel beads, and then add 400 μL of a methanol–water solution (4:1) containing 4 μg/mL l-2-chlorophenylalanine. After cooling the mixture at -40 °C for 2 min, grind the tissue thoroughly, perform ultrasonic extraction in an ice bath, and incubate the mixture at -40 °C for 2 h. Centrifuge the sample for 10 min, collect 150 μL of the supernatant, and filter it through a 0.22 μm organic phase syringe filter. Transfer the filtered supernatant to an LC injection vial and analyze it using a liquid chromatography-tandem mass spectrometry system comprising an ACQUITY UPLC I-Class plus and a QE high-resolution mass spectrometer. Process the data with Progenesis QI V2.3 software, using VIP > 1.0 and p-value < 0.05 to identify differential metabolites.

Dual-luciferase reporter assay

To investigate the c-MYC transcriptional regulation of Pfkfb3, clone the Pfkfb3 promoter into the pGL3 vector to construct the reporter gene vector.Clone the transcription factor into the pCDNA3.1 expression vector to generate the target gene expression vector. Transfect the experimental group with the reporter gene, target gene expression vector, TK vector, and the control group with the reporter gene, empty vector, TK vector into HEK293T cells. After incubation, lyse the cells and measure the firefly and Renilla luciferase activities using a spectrophotometer. Use Renilla luciferase activity as an endogenous control for normalization.

Chromatin immunoprecipitation (ChIP) assay

The ChIP assay was carried out per the kit's guide. For immunoprecipitation, an anti-c-MYC antibody (Cat# 18,583; 1:100, CST) was used. Additionally, purified DNA was analyzed by qPCR. Primer sequences: WT1 (F: GCC ATTCTGTCAGCACTTGG, R: CAGACCTTGTTG CCACTGAG), WT2 (F: GGAGAGAGGGAGGAAGGA GA, R: CCCAGACACAACAGAAGAGG), and WT3 (F: CAAAGGCATTCACCCCAAGA, R: CTGCCCTGG AACTCACTTT). The results of chromatin immunoprecipitation were analyzed using q-PCR and agarose gel electrophoresis.

Seahorse XF assays

Macrophages were seeded in XFe96 plates at a density of $1.2 \times 10^{\wedge}4$ cells per well. After allowing the cells to adhere at room temperature for 1 h on a clean bench, they were stimulated overnight with LPS (100 ng/ml). Concurrently, probe plates containing sterile water and calibration solution were placed in a 37 °C non-CO2 incubator overnight. The next day, the sterile water was discarded from the probe plates, and 200 μL of calibration solution was added. The plates were then incubated in the 37 °C non-CO2 incubator for 60 min.Mitochondrial stress test solutions (1 mM pyruvate, 2 mM glutamine, and 10 mM glucose) and glycolysis stress test solution (2 mM glutamine) were prepared separately. The cells were washed with the respective test solutions, and the cell culture

plates were incubated in the 37 °C non-CO2 incubator for 60 min.For the mitochondrial stress test, the following drug concentrations were used: Oligomycin (1.5 μM), Carbonyl cyanide-p-trifluoromethoxyphenylhydrazone (FCCP) (2 μM), and Rotenone/Antimycin A (0.5 μM), which were added to the respective ports of the utility plate. For the glycolysis stress test, the drugs used were Glucose (10 mM), Oligomycin (1.0 μM), and 2-DG (50 mM).First, run the probe plate on the Seahorse XF Pro Analyzer (Agilent, Lexington, MA) for calibration. After calibration, replace the hydration plate with the cell culture plate and run the real-time Seahorse XFe96 analyzer using the Wave software to analyze the data.

Macrophages were seeded in XFe96 plates at a density of 1.2×10^4 cells/well. After incubating at room temperature for 1 h on a clean bench until the cells adhered to the wall, they were stimulated overnight with LPS (100 ng/ml). At the same time, probe plates with sterile water and calibration solution were placed in a 37 °C non-CO_2 incubator overnight. The next day, the sterile water in the probe plate was discarded, and 200 ul of calibration solution was added and placed in a 37 °C non-CO_2 cell culture incubator for 60 min. Mitochondrial stress test solutions (1 mM pyruvate, 2 mM glutamine, and 10 mM glucose) and glycolysis stress test solution (2 mM glutamine) were prepared separately. The cells were washed with the test solutions as required. Then the cell culture plates were placed in a 37 °C non-CO_2 cell culture incubator for 60 min. According to the instructions, the drug concentrations in the mitochondrial stress test were Oligomycin (1.5 μM), Carbonyl cyanide-p-trifluoromethoxyphenylhydrazone (FCCP) (2 μM), and Rotenone/antimycin A (0.5 μM), added to the respective ports of the utility plate for the standard MitoStress test. The drug concentrations in the glycolysis stress test were Glucose (10 mM), Oligomycin (1.0 μM), and 2-DG (50 mM). First, run the probe plate on the Seahorse XF Pro Analyzer (Agilent, Lexington, MA) for calibration. After completion, replace the hydration plate with the cell culture plate, and run the real-time Seahorse XFe96 analyzer using the Wave software to analyze the data.

Enzyme-linked immunosorbent assay (ELISA)

The concentrations of TNF-α, IL-6, and IL-1β in mouse serum and macrophage culture supernatants were measured using ELISA kits (Cat#: E-EL-M3063, E-EL-M0044, E-EL-M0037, Elabscience) following the manufacturer's instructions.

Lactate assay, Nitric Oxide (NO) assay and ATP assay

According to the manufacturer's instructions, all detection of lysed cells will be normalized using BCA detection. Lactate assay kit (Cat# KTB1100, abbkine), NO assay kit (Cat# S0023, beyotime), and ATP assay kit (Cat# S0026B, beyotime).

2-NBDG, ROS (Reactive Oxygen Species), MitoSOX Red and Mito-Tracker Deep Red

According to the manufacturer's instructions, first treat the macrophages accordingly for 24 h, then wash them once with PBS. Add the diluted liquid prepared according to the instructions into the culture plate, and incubate it in the dark at 37 °C for the specified time. After that, gently transfer the cells into a flow tube, wash them twice with PBS, and use a flow cytometer for detection. Calculate the average fluorescence intensity for statistical analysis. 2-NBDG (Cat# GC10289, glpbio) should be incubated in the dark for 45 min, while ROS (Cat# S0033S, beyotime), MitoSOX Red (Cat# GC68230, glpbio), and Mito-Tracker Deep Red (Cat# C1035, beyotime) should all be incubated in the dark for thirty minutes.

Flow cytometry analysis

As previously reported, mouse spleens were separated and single-cell suspensions were prepared [37–39]. After the macrophages were treated, they were cleaned once with PBS, gently blown down to the flow tube, cleaned three times with PBS, and then disposed of with PBS. 100ul PBS was added, and 2ul Cd11b-APC (Cat# 101,212, Biolegend), F4/80-FITC (Cat# 123,108, Biolegend), and Cd86-PE (Cat# 105,008, Biolegend) were added to each flow tube respectively.

Annexin V-FITC/PI apoptosis assay

Apoptosis detection experiment (Cat# E-CK-A211, elabscience) was conducted according to the instructions. Cells were placed into a flow tube, centrifuged at 300×g for 5 min, and the supernatant was discarded. The cells were washed once with PBS, centrifuged, and the supernatant was discarded. 100 μL of diluted 1×Annexin V Binding Buffer was added to resuspend the cells. Then, 2.5 μL of Annexin V-FITC Reagent and 2.5 μL of PI Reagent were added to the cell suspension, and the mixture was incubated at room temperature in the dark for 20 min. Subsequently, 400 μL of diluted 1×Annexin V Binding Buffer was added before flow cytometry analysis.

Mitochondrial permeability transition pore assay

According to the manufacturer's instructions (Cat# KTA4002, abbkine), three types of detection solutions should be prepared: Calcein AM staining solution and Ionomycin control solution are only used for preliminary experiments to verify the staining conditions. The Fluorescence quenching solution working fluid is used in the formal experiment to measure the detection solution of

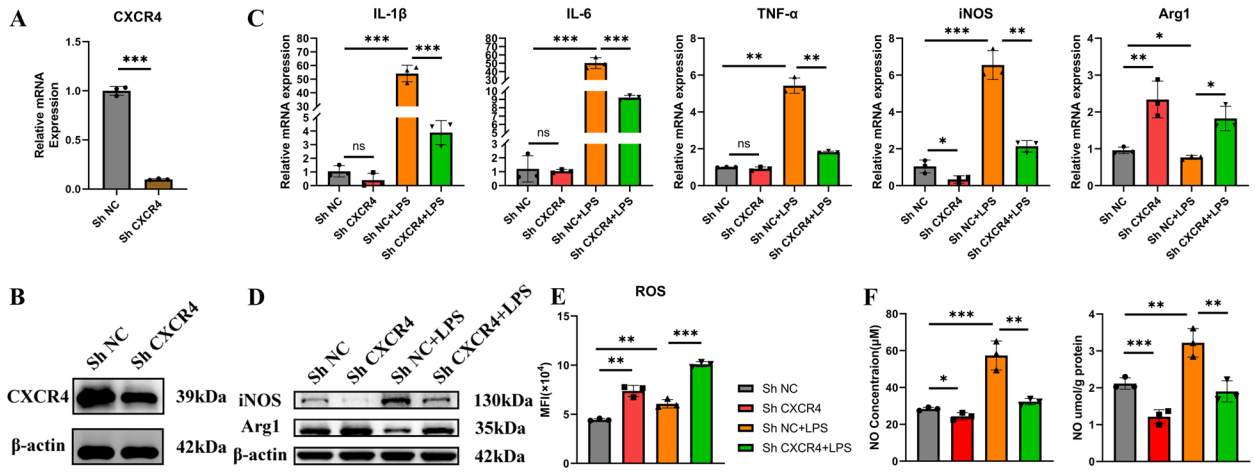

Fig. 1 Silencing CXCR4 alleviates M1 polarization of macrophages and reduces their inflammatory capacity. The efficiency of knocking down CXCR4 in macrophages was detected by PCR **A** and WB **B**. Divide macrophages into ShNC, Sh CXCR4, Sh NC + LPS, and Sh CXCR4 + LPS four groups. The mRNA expression levels of IL-1β, IL-6, TNF-α, iNOS and Arg1 in CXCR4-knockdown macrophages were analyzed by PCR **C** and in protein expression levels of iNOS and Arg1 **D**. **E** The ROS levels in macrophages were detected by flow cytometry. **F** Detect the content of NO in the supernatant and intracellular of four sets of macrophage culture medium. respectively. ns, Not Significant. ***$p < 0.001$, **$p < 0.01$, *$p < 0.05$

MPTP. Follow the experimental procedures as required, and calculate the average fluorescence intensity using a flow cytometer for statistical analysis.

Statistical analysis

R-4.2.3 software, SPSS 26.0 software, image J software and GraphPad Prism 8.0 software were used for statistics. Data were expressed as the mean value ± SD. Student t test and Wilcoxon rank sum test were used for statistical analysis. A p value < 0.05 was considered statistically significant.

Results

Silencing CXCR4 alleviates M1 polarization of macrophages and reduces their inflammatory capacity

First, we verified the expression of CXCR4 in lentivirus-silenced macrophages using PCR and WB (Fig. 1A and B, Figure S1A). For M1 marker genes, we found that the decreased expression of CXCR4 led to a reduction in IL1β, IL6, TNF-α, and iNOS expression, while increasing ARG1 expression (Fig. 1C). Therefore, we detected that silencing CXCR4 under LPS stimulation can reduce the secretion of inflammatory factors in the cell culture medium (Figure S1B).This was further confirmed by WB experiments (Fig. 1D and Figure S1C). Similar we obtained consistent Western blot results by downregulating CXCR4 with small interfering RNA in mouse bone marrow-derived macrophages (Figure S1D and E).Since the pro-inflammatory capacity of M1-polarized macrophages mainly depends on the flux of glucose to lactate, the production of reactive oxygen species, and nitric oxide [40]. So we tested the impact of CXCR4 on ROS (Fig. 1E) and NO production (Fig. 1F) in macrophages. Consistent with the above, whether macrophages were induced to M1 polarization by LPS or not, both the content of NO in the cell culture medium and inside the cells was decreased. However, ROS levels were abnormally elevated, which seems to contradict the trend of M1 metabolic reprogramming, as for many years, reactive oxygen species have been viewed as destructive molecules and byproducts of cell stress. However, recent literature research indicates the importance of ROS as important endogenous signaling molecules [40–42]. The main sources of ROS are NADPH oxidase (NOX) and mitochondria [43]. The main source of ROS in macrophages is REDOX reaction resulting from electron transfer by mitochondrial complex [44]. Therefore, next, we would like to elaborate the effects of CXCR4 on mitochondria and metabolic processes of macrophages.

Inhibiting CXCR4 does not decrease macrophage mitochondrial function, but enhances mitochondrial metabolism

We used MitoSOX reagent to observe the distribution of mitochondrial ROS, which was consistent with the previous findings that the reduction of CXCR4 led to an increase in mitochondrial ROS (Fig. 2A). We hypothesized whether this was due to an increase in mitochondrial function and metabolism, or due to mitochondrial dysfunction (respiratory chain dysfunction, inner membrane damage, changes in membrane permeability) leading to increased ROS. The Mito-Tracker Red CMXRos probe can specifically detect bioactive mitochondria and monitor mitochondrial membrane potential.

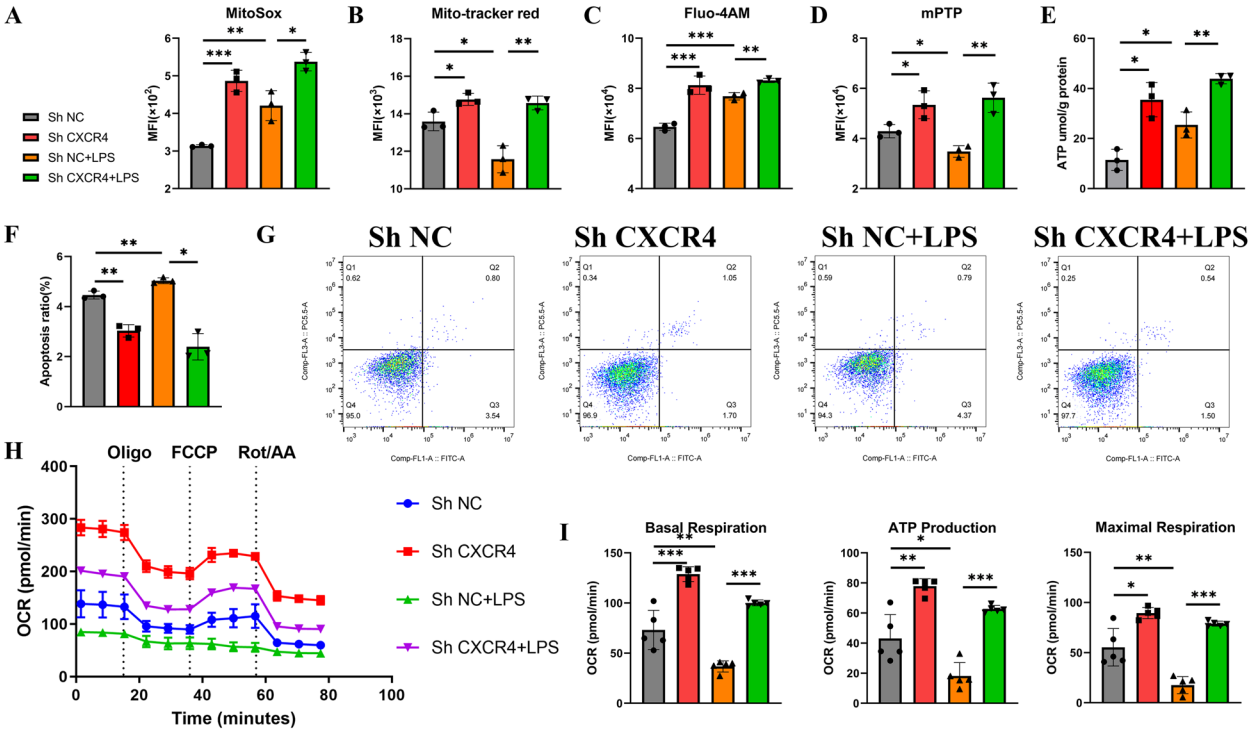

Fig. 2 Inhibiting CXCR4 does not decrease macrophage mitochondrial function, but enhances mitochondrial metabolism. The experimental groups of macrophages are ShNC, Sh CXCR4, Sh NC + LPS, and Sh CXCR4 + LPS. A-D were used for flow cytometry to detect mitosox **A**, mito-tracker red **B**, Fluo-4AM **C**, and Mptp **D**. **E** ATP content in macrophages was measured using BCA for normalization. Apoptosis rate of macrophages was detected by flow cytometry, **F** corresponding data analysis was performed based on the apoptosis data, **G** flow cytometry graphs of cells. **H** Mitochondrial metabolic function of ibmdm was determined by real-time recording mitochondrial pressure (OAR) after continuous injection of oligomycin (O), FCCP, and Rot/AA. **I** Data from (H) was used to calculate basal respiratory capacity, ATP production, and maximum respiratory capacity of mitochondria. ns, Not Significant. ***$p < 0.001$, **$p < 0.01$, *$p < 0.05$

Experimental data showed that CXCR4 did not decrease mitochondrial membrane potential and, under LPS-induced conditions, to some extent, protected mitochondrial function (Fig. 2B). The concentration of intracellular calcium ions affects mitochondrial function, including the transport of tricarboxylic acid cycle proteins, membrane permeability, and apoptosis. Experimental data showed that although calcium ion levels increased (Fig. 2C), there was also a decrease in the opening of mitochondrial permeability transition pores (Fig. 2D). Typically, a decrease in ATP levels indicates impaired or decreased mitochondrial function. In apoptosis, a decrease in ATP levels usually occurs simultaneously with a decrease in mitochondrial membrane potential. In this experiment, CXCR4 did not reduce intracellular ATP content (Fig. 2E). Moreover, the impact of CXCR4 deficiency on macrophage mitochondrial function was evident in our in vitro studies using bone marrow-derived macrophages, with results consistent with our expectations (Figure S1 E–G). Mitochondria act as "signal amplifiers" for cell apoptosis, influencing apoptosis by regulating the oxidative state within the cell and interacting with the endoplasmic reticulum to jointly modulate this process [45, 46]. Based on this, we explored the apoptotic state of cells, and CXCR4 was found to alleviate LPS-induced apoptosis (Fig. 2F and G). Finally, using the Seahorse XF96 extracellular flux analyzer, we measured the OCR (oxygen consumption rate, representing OXPHOS) levels of macrophages. Under LPS-induced polarization conditions, CXCR4 still played a protective role in mitochondrial function (Fig. 2H). ATP production, mitochondrial basal metabolism, and maximum metabolism levels also increased with the silencing of CXCR4 (Fig. 2I). Importantly, the significant reduction of CXCR4 enhanced the OCR of maximum and basal respiration weakened by LPS, indicating a protective role of CXCR4 in mitochondria. As for the changes in intracellular calcium ion concentrations, we speculate that CXCR4 itself affects the activation of calcium ion channels or the intracellular calcium ion homeostasis.

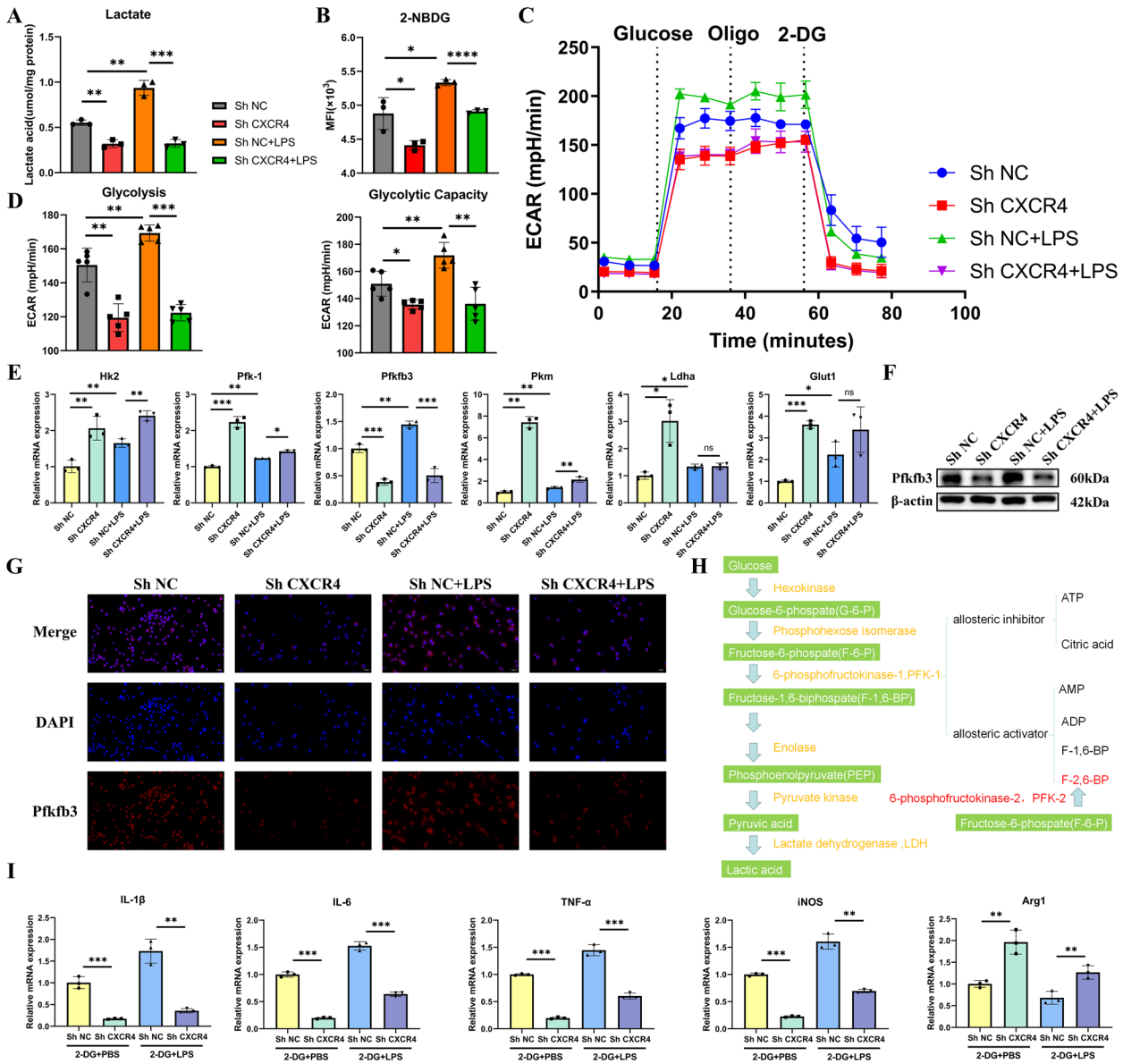

Fig. 3 Inhibit CXCR4 and reduce macrophage glycolytic metabolism. Macrophages are divided into four groups: Sh NC, ShCXCR4, Sh NC + LPS, and Sh CXCR4 + LPS. **A** Measurement of lactate production in iBMDM in response to LPS and CXCR4. **B** Flow cytometry analysis to assess cellular glucose uptake capacity. **C** Following sequential injections of glucose (Glc), oligomycin (O), and 2DG, changes in glycolytic stress in iBMDM are determined by real-time recording of extracellular acidification rate (ECAR). **D** Data analysis from (**C**) to determine the ECAR rate and maximum glycolytic capacity of macrophages. **E** q-PCR analysis to detect changes in mRNA levels of key glycolytic enzymes in macrophages. **F** Western blot analysis to determine the expression of Pfkfb3 in macrophages after knocking down CXCR4. **G** Immunofluorescence staining to observe the localization and changes in the levels of Pfkfb3 in macrophages. **H** a simple flow chart of glycolytic metabolism. **I** Transfect iBMDMs with Sh NC and Sh CXCR4, treat with LPS (100 ng/mL) for 4 h. Wash the cells three times, pre-treat with 2.5 mM 2-DG for 1 h, then treat with or without LPS (100 ng/mL) for another 4 h. Determine the mRNA levels of IL-1β, IL-6, TNF-α, iNOS, and Arg1.ns, Not Significant. ***$p < 0.001$, **$p < 0.01$, *$p < 0.05$

Inhibit CXCR4 and reduce macrophage glycolytic metabolism

During the polarization process of M1 macrophages, glycolysis metabolism plays a dominant role [47, 48]. Decreasing CXCR4 can enhance the mitochondrial metabolism of macrophages. Based on this, we speculate that CXCR4 can alter macrophage polarization status through glycolysis metabolism. Cellular lactate levels (Fig. 3A) and glucose uptake experiments (Fig. 3B) indicated that inhibition of CXCR4 was associated with a suppression of glycolytic flux in macrophages. Consistent with expectations, Seahorse

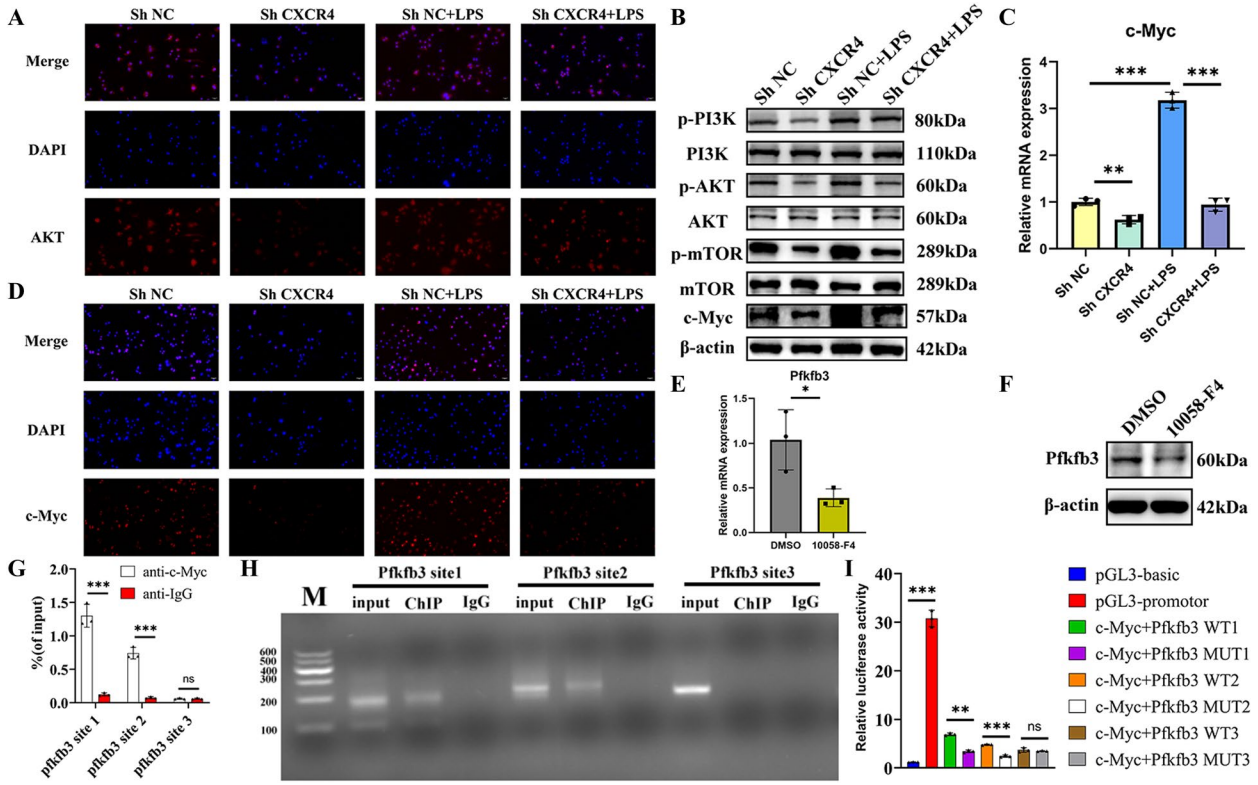

Fig. 4 CXCR4 affects c-Myc transcription regulation through the PI3K/AKT/mTOR pathway. **A** Immunofluorescence staining showed changes in AKT in four groups of macrophages. **B** WB analysis of changes in the PI3K/AKT/mTOR pathway and phosphorylation, as well as c-Myc in macrophages. **C** PCR analysis of mRNA c-Myc changes after knocking down CXCR4. **D** Immunofluorescence staining analysis of changes in the localization and content of c-Myc. PCR **E** and WB **F** analysis of Pfkfb3 changes after using c-Myc (10,058-F4). To verify the transcriptional regulation of c-Myc on Pfkfb3. **G** ChIP-qPCR detection of the binding status of c-Myc to three sites on the Pfkfb3 promoter. **H** Agarose gel electrophoresis results of PCR products further elucidated the transcriptional binding of c-Myc to Pfkfb3. **I** Plasmid transfection in 293 T cells, dual-luciferase assay to clarify the interaction of the transcription factor c-Myc with the target gene Pfkfb3. ns, Not Significant. ***$p < 0.001$, **$p < 0.01$, *$p < 0.05$

glycolytic stress tests revealed that LPS stimulation for 24 h shifted macrophages towards anaerobic glycolysis, and inhibition of CXCR4 led to a decrease in ECAR in the presence of glucose (Fig. 3C). Similarly, conversely, silencing CXCR4 reduced baseline glycolysis and significantly impaired the ability of glycolysis to increase after mitochondrial inhibition (Fig. 3D). Figure 3E shows the changes in several key enzymes of glycolysis after reducing CXCR4 expression, with only Pfkfb3 being downregulated. We validated the changes of Pfkfb3 at the protein level (Fig. 3F and Figure S2A). PFKFB3 is also inhibited in BMDM cells with CXCR4 inhibition (Figure S1E).Immunofluorescence staining showed that the expression of Pfkfb3 in macrophages, whether polarized or not, was influenced by CXCR4 (Fig. 3G). Figure 3H shows the main enzymes involved in the glycolysis process and regulatory enzymes. Phosphofructokinase-1 is the most important enzyme in regulating glycolytic rate, and its most potent allosteric activator is fructose-2,6-bisphosphate, which is formed by catalyzing fructose-6-phosphate-C2 phosphorylation by phosphofructokinase-2 [49]. We used the glycolytic inhibitor 2-deoxy-D-glucose (2-DG) to block glucose supply and found that in macrophages with inhibited CXCR4 expression, the expression of IL-1β, IL-6, TNF-α, and iNOS decreased while arginase-1 increased (Fig. 3I). These results indicate that CXCR4 can alter macrophage polarization by affecting glycolytic metabolism processes.

CXCR4 affects c-Myc transcription regulation through the PI3K/AKT/mTOR pathway

AKT pathway and c-Myc are major transcription factors deeply involved in glycolytic metabolism [50–52], We want to explore whether CXCR4 downstream affects the expression of AKT and c-Myc. Immunofluorescence staining shows that CXCR4 reduction in macrophages leads to decreased AKT pathway activation (Fig. 4A). Figure 4B and Figure S2B indicates changes in the activation of the PI3K/AKT/mTOR pathway and

c-myc protein expression. CXCR4 expression affects mRNA c-Myc expression (Fig. 4C). c-Myc is distributed less in the cytoplasm and nucleus of macrophages with silenced CXCR4 (Fig. 4D). We used a c-Myc inhibitor (10,058-F4) and found that Pfkfb3 expression is reduced (Fig. 4E and F and Figure S2C). Firstly, through ChIP experiments, we verified the predicted binding sites 1 and 2, where c-Myc as a transcription factor can bind to the promoter region of Pfkfb3, as shown by q-PCR (Fig. 4H) and gel electrophoresis (Fig. 4G). Subsequently, we designed plasmids targeting three sites for dual-luciferase experiments to demonstrate that c-Myc can regulate the expression of Pfkfb3 (Fig. 5I). To further elucidate the function of Pfkfb3, we silenced Pfkfb3 and subsequently examined the polarization levels and glycolytic capacity of macrophages. The results aligned with our previous data (Figure S2D-G). All these results confirm that CXCR4 induction of Pfkfb3 is crucial for M1 polarization, glycolysis, and inflammation.

M1 cells expressing CXCR4 + are highly expressed in prostatitis tissues

We collected human surgical specimens of prostate hyperplasia and divided them into inflammatory group and non-inflammatory group based on whether there

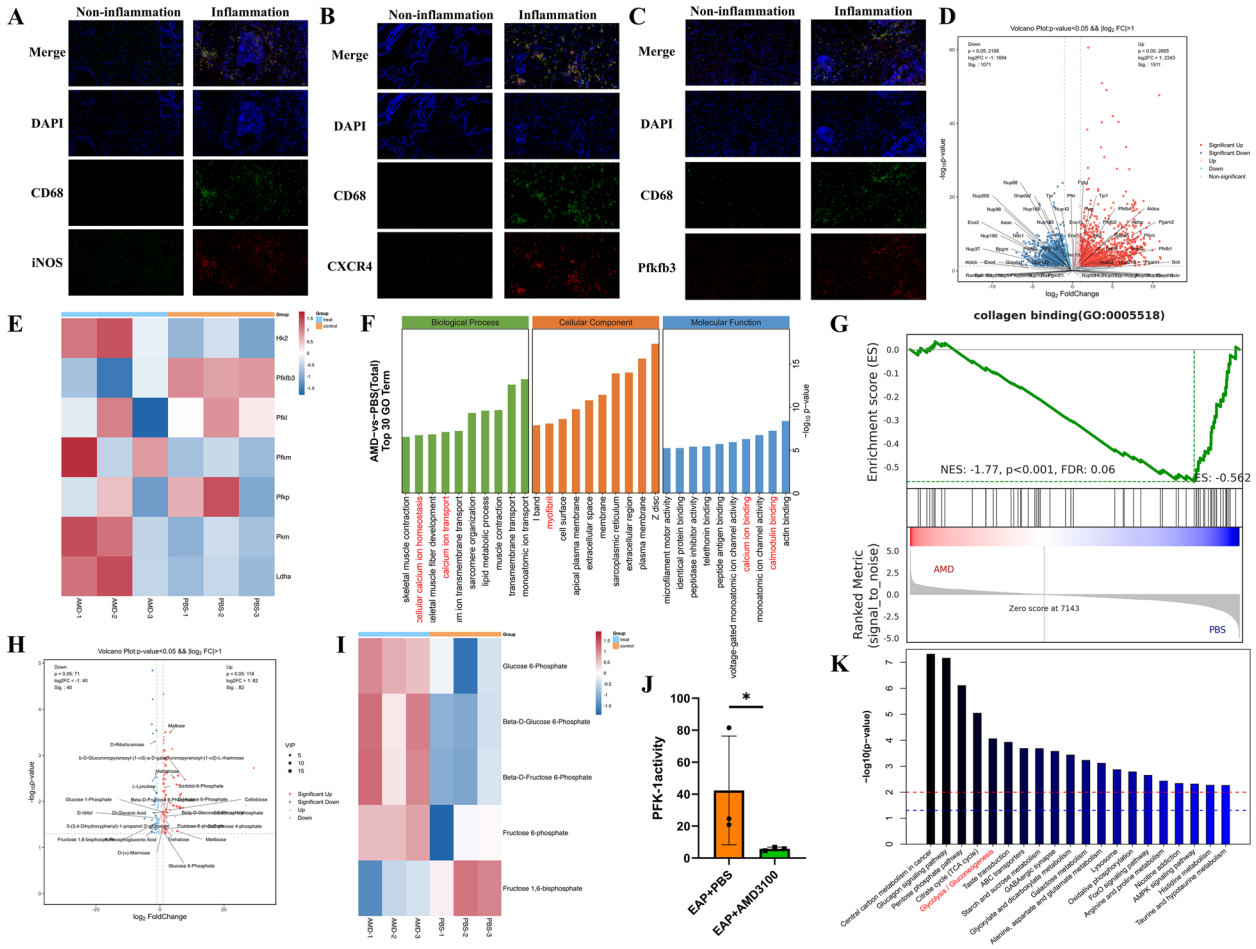

Fig. 5 M1 cells expressing CXCR4 + are highly expressed in prostatitis tissues. We divided the collected human prostate tissues into inflammatory group and non-inflammatory group, and conducted immunofluorescence co-localization of CD68/iNOS **A**, CD68/CXCR4 **B**, and CD68/Pfkfb3 **C**. We established EAP mice and injected AMD3100 (5 mg/kg/d) into the abdominal cavity, with the control group receiving an equal amount of PBS injection. After sacrificing the mice, we took half of the prostate for RNA-seq and non-targeted metabolic sequencing. **D** The volcano plot shows gene changes involved in glycolytic metabolism in RNA-seq. **E** The heatmap displays the mRNA levels of key glycolytic enzymes in each sample. **F** GO enrichment analysis of differentially expressed genes pathways. **G** GSEA enrichment analysis of different pathways. **H** The volcano plot shows differential metabolites in the non-targeted metabolic group. **I** The heatmap displays the levels of products in glycolysis process in each sample. **J** Analysis of PFK-1 enzyme activity after AMD3100 use. **K** KEGG enrichment analysis of differential pathways of metabolic products. ns, Not Significant. *$p < 0.05$

was a large amount of inflammatory cell infiltration in the pathology. Immunofluorescence co-staining of CD68 and iNOS indicated that prostate inflammation had more M1 cell infiltration (Fig. 5A). Immunofluorescence localization of CD68 with CXCR4 and PFKFB3 showed that the expression of CXCR4 and PFKFB3 in prostate macrophages with inflammation was higher (Fig. 5B and C). We also found that tissues exhibiting more severe inflammation in humans showed higher expression of CXCL12 (Figure S3A). Therefore, we reasonably speculated that CXCR4-driven M1 macrophages in prostate inflammation may influence the pathological process to a certain extent. In order to explore possible mechanisms, we constructed a mouse model of experimental autoimmune prostatitis (EAP) and continuously intraperitoneally injected AMD3100 (CXCR4 inhibitor) at a dose of 5 mg/kg/day for two weeks, while the control group received an equal amount of PBS intraperitoneally. After sacrificing the mice, we took half of the prostate tissue from each group for RNA-seq and untargeted metabolomics sequencing. Figure 5D displayed the distribution of genes involved in glycolytic metabolism with $|\text{LogFc}|>1$ and $p<0.05$ as the criteria through a volcano plot, indicating that most key genes involved in glycolysis were upregulated or unchanged, while Pfkfb3 was downregulated. The heatmap showed the expression levels of key glycolytic metabolism enzymes in each group (Fig. 5E). GO enrichment analysis revealed differences in terms of myofibril and calcium ion pathways (Fig. 5F). In the GSEA analysis, the collagen binding pathway was significantly inhibited after the use of AMD3100 (Fig. 5G). The sequencing results of the transcriptome indicated that CXCR4 might affect the process of prostate fibrosis. As for untargeted metabolomics, we focused on changes in carbohydrate metabolism products. We first showed the differences in related metabolites (Fig. 5H). Then, in the order of glycolytic metabolism process, we sequentially displayed the levels of products through a heatmap. We could clearly see that, including fructose-6-phosphate, the increase in glycolytic products in inflammation could not be changed by the use of AMD3100 (Fig. 5I). The change occurred in the process from fructose-6-phosphate to fructose-1,6-diphosphate, a step catalyzed by the key enzyme Pfk-1. The expression of Pfkm was increased in the transcriptome (Fig. 5E), but the expression of Pfkfb3 was decreased. Pfkfb3 catalyzes fructose-2,6-diphosphate, the most important regulator of Pfk-1, deeply affecting the flux of sugar metabolism [49]. The ratio of Fructose 6-phosphate to Fructose 1,6-bisphosphate is used to demonstrate the activity of the Pfk-1 enzyme. It is evident that Pfk-1 activity significantly decreases after the use of AMD3100 (Fig. 5J). As expected, KEGG analysis of the final metabolism pathway shows differences in glycolysis metabolism pathway after the use of AMD3100 (Fig. 5K).

Inhibiting CXCR4 expression alleviates the severity of chronic prostatitis in mice and reduces macrophage infiltration

We first constructed an adenovirus-related virus knockdown CXCR4 mouse model, and then constructed an EAP model. HE staining and immunohistochemical staining of CD45 showed that mouse inflammation decreased with the decrease of CXCR4, as well as a reduction in the infiltration of inflammatory cells in the stroma (Fig. 6A). The inflammatory scores from the HE staining (Fig. 6B) and the mouse pelvic pain test (Fig. 6C) also indicated relief of inflammation. Figure 6D and Figure S3B illustrates the decrease in CXCR4. The mRNA levels of inflammatory factors including IL-1β, IL-6, and TNF-α in prostate tissue decreased with the inhibition of CXCR4 (Fig. 6E). The protein content of inflammatory factors in the mouse serum is consistent (Figure S3C). Immunofluorescence staining demonstrated the impact of CXCR4 on macrophage infiltration in prostatitis (Fig. 6F). The proportion of M1 cells in mice with prostatitis detected by flow cytometry in vivo, we found that the proportion of M1 cells increased when inflammation occurred and decreased with the reduction of CXCR4(Fig. 6G). The results of IHC showed that Pfkfb3 decreases in prostatitis with the decrease of CXCR4 (Fig. 6H), which was also validated by WB experiments (Fig. 6I and Figure S 3D).

Reducing CXCR4 can inhibit chronic prostatitis fibrosis

Figure 7A shows that the degree of prostate fibrosis in EAP + shCXCR4 mice is significantly lower than in EAP + shNC mice, as demonstrated by Masson, Sirius Red, and α-smooth muscle actin (α-SMA) staining. On the day of sacrificing the mice, we measured the body weight and prostate weight, and calculated the prostate fibrosis index as prostate weight/body weight ratio. The fibrosis index of the prostate in the EAP + shCXCR4 mouse group decreased compared to the control group (Fig. 7B). Immunofluorescence staining showed a decrease in collagen I (Fig. 7C) in the prostate tissue of EAP + shCXCR4 mice. Furthermore, the mRNA expression of α-SMA, Col1a1, and Timp1 in the prostate tissue of EAP + shCXCR4 mice was significantly lower than in the control group (Fig. 7D). Western blot analysis further showed that CXCR4 deficiency reduced the expression of type I collagen, α-SMA, and Timp1 in fibrotic prostate tissue compared to the control group (Fig. 7E and Figure S4 A). To clarify the impact of macrophages on fibroblasts, we conducted a co-culture experiment following the process shown

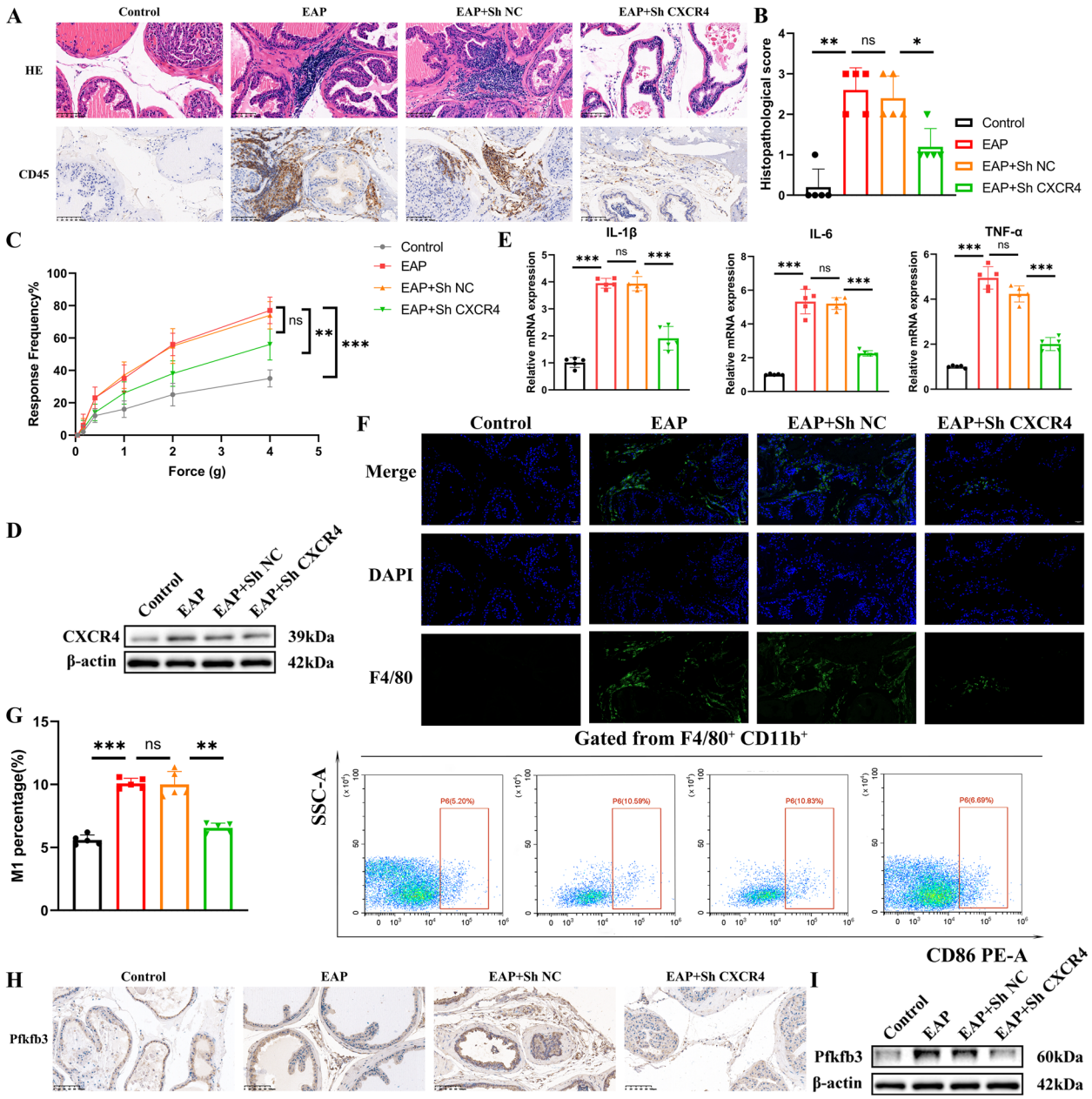

Fig. 6 Inhibiting CXCR4 expression alleviates the severity of chronic prostatitis in mice and reduces macrophage infiltration. First inject adenovirus into the tail vein of the mice to construct the EAP mouse model, divided into four groups: control, EAP, EAP + Sh NC, and EAP + Sh CXCR4. **A** Show the inflammation status of the four groups of mice through HE staining and immunohistochemistry of CD45. **B** Quantify the degree of inflammation in mice through HE inflammatory scoring. **C** Pelvic pain stimulation experiment, indicating that inhibiting CXCR4 can alleviate pelvic pain symptoms in EAP mice. **D** WB analysis of the content of CXCR4 protein in mouse prostate. **E** PCR analysis of the expression of IL-1β, IL-6, and TNF-α mRNA in mouse prostate tissue. **F** Immunofluorescence staining analysis of macrophage infiltration in the prostate. **G** Flow cytometry results of splenic macrophages from each group of mice. **H** Immunohistochemistry staining of Pfkfb3 expression and distribution in the prostate. **I** WB analysis of the expression of Pfkfb3 in mouse prostate. ns, Not Significant. ***$p < 0.001$, **$p < 0.01$, *$p < 0.05$

in Fig. 7F. Macrophages were polarized by LPS induction in vitro, and then the polarized macrophages were used to activate fibroblasts. PCR results showed that M1 macrophages with reduced CXCR4 had decreased levels of three fibrosis markers (α-SMA, Col1a1, and Timp1) compared to M1 macrophages in the control Sh NC group (Fig. 7G). Immunofluorescence staining showed a significant reduction in the distribution of

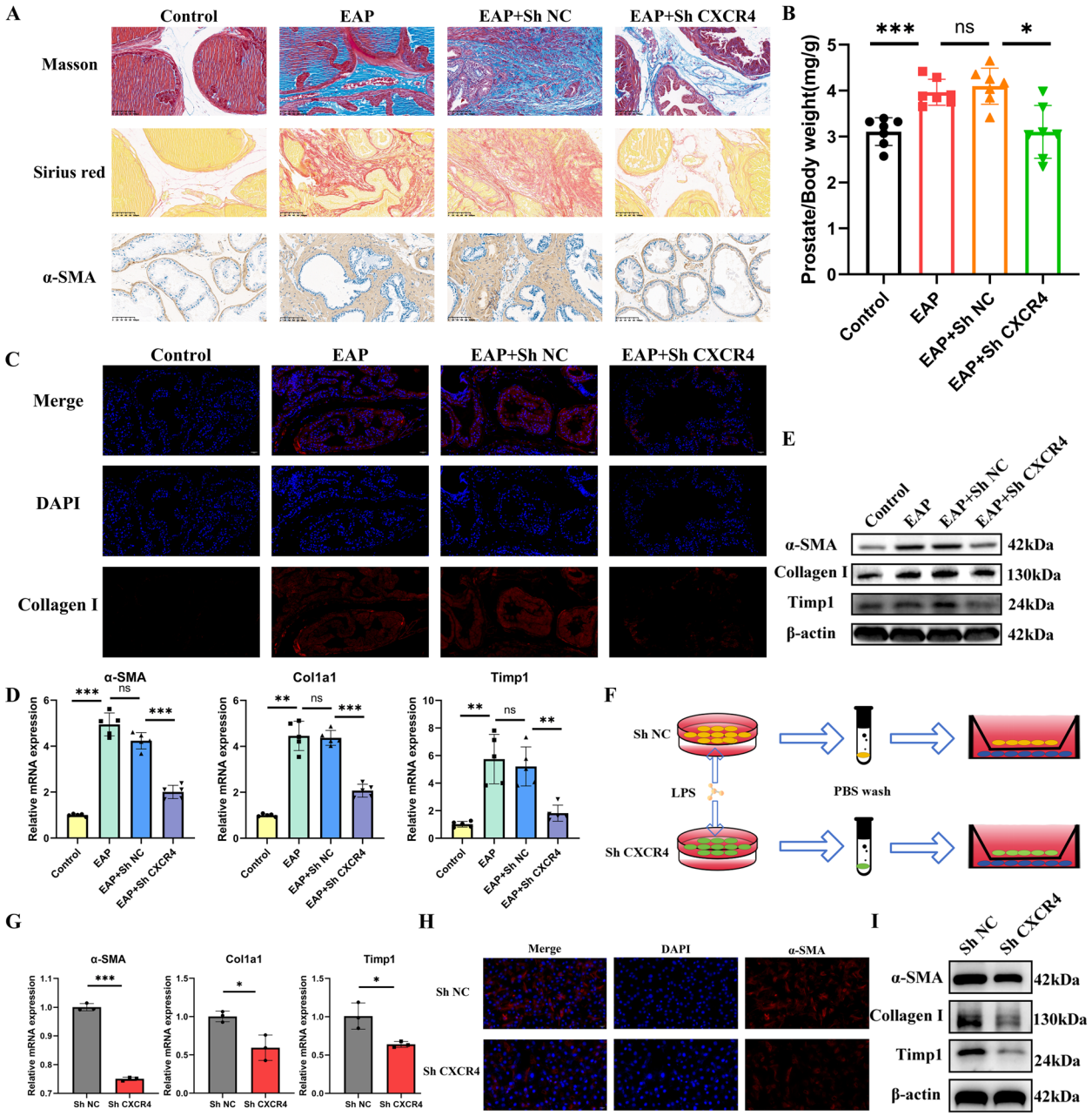

Fig. 7 Reducing CXCR4 can inhibit chronic prostatitis fibrosis. The mouse prostate fibrosis is divided into four groups: control, EAP, EAP + Sh NC, and EAP + Sh CXCR4. **A** Masson staining, Sirius Red staining, and immunohistochemistry α-SMA staining were performed to clarify the situation of prostate fibrosis. **B** The ratio of mouse prostate weight/body weight was used to assess prostate fibrosis. **C** Immunofluorescence staining analyzed the changes of collagen 1 in the prostate. **D** PCR analysis of changes in α-SMA, Col1a1, and Timp1 mRNA in fibrotic mouse prostate. **E** WB analysis of changes in α-SMA, collagen 1, and Timp1 in fibrotic mouse prostate. **F** Schematic diagram of the co-culture process of macrophages and fibroblasts to clarify the effect of knocking down CXCR4 on M1 macrophage activation of fibroblasts. **G** Changes in α-SMA, Col1a1, and Timp1 mRNA in fibroblasts. **H** Immunofluorescence staining analyzed the changes of α-SMA in fibroblasts. **I** WB analysis of changes in α-SMA, Collagen 1, and Timp1 in fibroblasts. ns, Not Significant. ***$p < 0.001$, **$p < 0.01$, *$p < 0.05$

α-smooth muscle actin, a major substance in fibrosis, in the knockdown CXCR4 group (Fig. 7H). Western blot analysis further indicated that CXCR4 deficiency weakened the activation of macrophages into fibroblasts and reduced the expression of type I collagen, α-SMA, and Timp1 (Fig. 7I and Figure S4 B). In addition, after treating EAP mice with 3PO, a PFKFB3 inhibitor, we observed a significant reduction in fibrosis within the

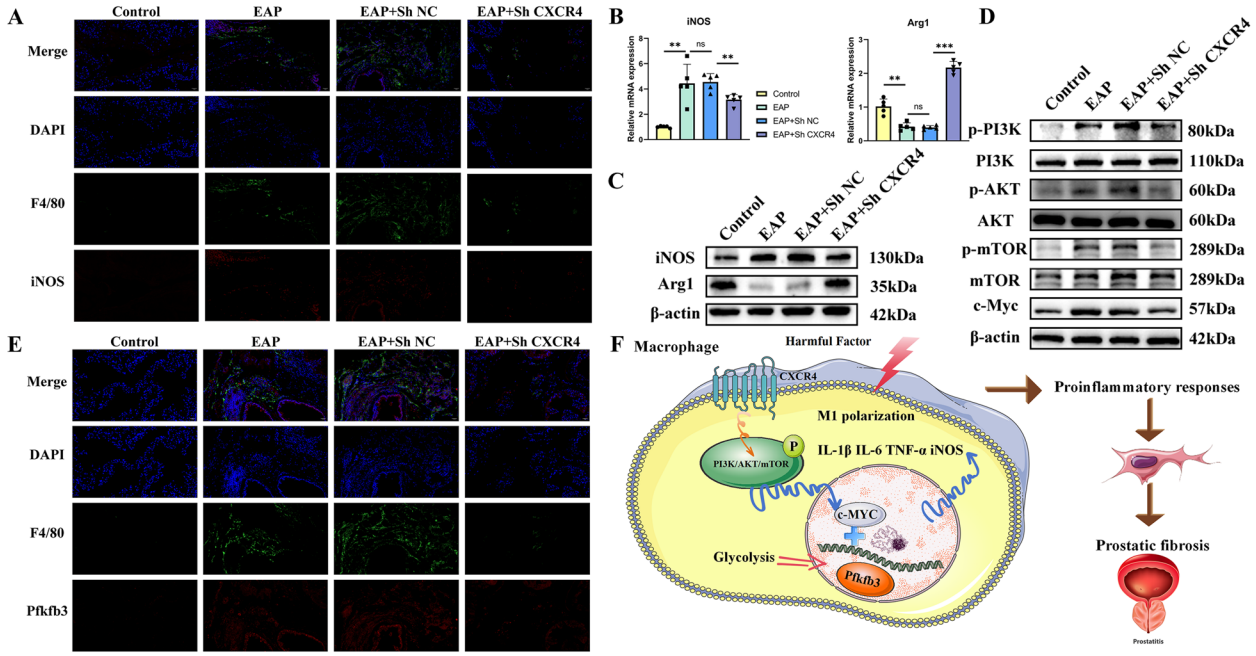

Fig. 8 CXCR4 deficiency alleviates M1 polarization and PI3K/AKT/mTOR pathway activation in fibrotic prostate. The mouse prostate fibrosis is divided into four groups: control, EAP, EAP + Sh NC, and EAP + Sh CXCR4. **A** Immunofluorescence co-staining analysis of the co-expression of F4/80/iNOS in prostate tissue. PCR (**B**) and WB (**C**) were used to detect the mRNA expression of iNOS and Arg1 in prostate tissue. **D** WB was employed to detect the phosphorylation activation of the PI3K/AKT/mTOR pathway and changes in the c-Myc protein level in prostate tissue. **E** Immunofluorescence staining analysis of the co-localization of F4/80/Pfkfb3 in prostate tissue. **F** Schematic diagram illustrating how CXCR4 influences c-Myc transcriptional regulation of Pfkfb3, leading to metabolic changes in macrophages and affecting the process of prostate fibrosis. ns, Not Significant. ***$p < 0.001$, **$p < 0.01$, *$p < 0.05$

prostate tissue (Figure S4C). Fibrotic markers were assessed at both the mRNA (Figure S4D) and protein (Figure S4E) levels in the prostate tissue of EAP mice treated with 3PO. The results indicated that PFKFB3 inhibition alleviates fibrosis in the prostate tissue of these mice. Our study results suggest that the lack of CXCR4 can reduce fibroblast activation and alleviate prostatic fibrosis in mice.

CXCR4 deficiency alleviates M1 polarization and PI3K/AKT/mTOR pathway activation in fibrotic prostate

As mentioned above, the lack of CXCR4 can alleviate liver inflammation, and CXCR4 may promote M1 polarization. We first immunofluorescence quantified M1, and the results showed that the iNOS + F4/80 + macrophages observed in EAP + Sh CXCR4 mice were fewer than those in EAP + Sh NC mice (Fig. 8A). In addition, in EAP mice with reduced CXCR4, the expression of inducible nitric oxide synthase (iNOS) mRNA was downregulated, while Arg1 was upregulated in the fibrotic prostate (Fig. 8B). WB analysis showed that in fibrotic prostates lacking CXCR4, the expression of iNOS and Arg1 was reduced compared to the control prostates (Fig. 8C and Figure S5A). There are numerous literature studies indicating that the PI3K/AKT/mTOR pathway in macrophages mediates the progression of many inflammatory diseases [53–55], and WB analysis in fibrotic prostates also showed significant inhibition of the AKT pathway by inhibiting CXCR4(Fig. 8D and Figure S5B). Finally, our immunofluorescence staining localization showed a decrease in the expression of Pfkfb3 in macrophages in fibrotic prostatitis (Fig. 8E). These results indicate that CXCR4 through the PI3K/AKT/mTOR pathway is a distinct regulatory pathway for macrophage-mediated chronic prostatitis.

Discussion

Chronic prostatitis is a complex multifactorial disease characterized by infiltration of various immune cells [12]. Derived from the bone marrow and infiltrating tissues, macrophages are a branch of mononuclear phagocytes that play a crucial role in maintaining the balance of tissue inflammation and immune attacks. When stimulated by tissue damage, macrophages are activated and polarized, secreting a large amount of pro-inflammatory and pro-fibrotic cytokines, and producing ECM components and other harmful molecules [19, 56, 57]. In this study, we identified CXCR4 as a pro-polarization molecule for

macrophages, which affects macrophages' impact on the fibrotic pathological process by regulating glucose metabolism. Furthermore, we elucidated the transcriptional activation of Pfkfb3 by c-MYC, thereby influencing the infiltration and polarization status of macrophages in the prostate. Our findings suggest for the first time that CXCR4 can alter macrophage metabolism processes and that macrophages are one of the main sources promoting prostate fibrosis in chronic prostatitis.

Our previous research aimed to explore potential genes influencing the occurrence and development of chronic prostatitis. During the sequencing of prostate tissues, we found abnormally elevated expression of CXCR4. Subsequent experiments confirmed that inhibiting CXCR4 with AMD3100 and silencing CXCL12 could significantly alleviate inflammation in vivo. However, the specific mechanism of action of CXCR4 in chronic prostatitis has not been fully discussed and studied [58].CXCR4 was originally isolated and purified from a human blood mononuclear cell gene library using gene probes, and it is highly expressed in mononuclear cells [59]. The research on CXCR4 related to macrophages has previously included studies on how CXCR4 affects the autophagy process in coronary heart disease [60], Liver damage affects macrophage apoptosis through CXCR4 [61] and macrophages in gastric cancer rely on CXCR4 to promote tumor metastasis [62] etc. Research on macrophages in chronic prostatitis has yielded clear results [38, 63]. In this study, we first clarified the influence of CXCR4 on the polarization state of macrophages. In the process of reducing the expression of CXCR4, we found that inflammatory factors, the proportion of M1 cells and the content of NO were decreased, but ROS was slightly increased. ROS mainly comes from mitochondria, and the rise of ROS is generally considered to be the destruction of mitochondrial function and electron leakage [64]. Based on this, we speculate that it is not the destruction of mitochondria, but the enhancement of oxidative phosphorylation that leads to the increase in ROS.

The PI3K/AKT signaling pathway is widely involved in cell growth, metabolism, apoptosis, and migration, and is closely related to the occurrence and development of inflammation [65, 66]. Activation of mTOR may promote the production of pro-inflammatory cytokines and dysregulate lipid and glucose metabolism [67]. Research has shown that under the regulation of multiple upstream factors, targeting the PI3K/AKT signaling pathway can effectively inhibit the M1 polarization of macrophages, thereby alleviating diseases such as osteoarthritis [68], gout [68], autoimmune hepatitis [69], and atherosclerosis [70] etc. However, the mechanism by which CXCR4 regulates macrophages to participate in the regulation of CNP through the PI3K/AKT signaling pathway remains unclear. In this study, the loss of CXCR4 inhibited the PI3K/AKT/mTOR pathway, thereby reducing the M1 polarization level in macrophages. In this process, AKT plays an important role by regulating glycolytic metabolism. In conclusion, these results suggest that CXCR4-mediated AKT activation may play a critical role in macrophage polarization and EAP fibrosis pathways.

The transition of macrophages from M1 to M2 status is characterized by a shift from glycolysis to oxidative phosphorylation [71]. This study provides compelling evidence that silencing CXCR4 does not impair mitochondrial function. Our data clearly show that while mitochondrial ROS levels increase, mitochondrial function remains intact. Glucose uptake experiments, lactate measurements, and Seahorse energy metabolism assays demonstrate that downregulation of CXCR4 is associated with inhibition of glycolysis and enhancement of mitochondrial function, which indirectly confirms that CXCR4 influences the polarization of macrophages towards the M1 state.As a key regulatory factor of glycolysis [72], The rate of glycolysis flux is determined by three key enzymes regulated under various conditions. Among them, the most crucial one is phosphofructokinase-1 (PFK-1), and its most important and potent allosteric regulator is fructose-2,6-bisphosphate, which negates the inhibitory effects of ATP and citrate [49]. In macrophages, the typical types are LPS-induced M1 macrophages and IL-4 and IL-13-induced M2 macrophages. Metabolic changes similar to the Warburg effect occur in the context of inflammation induction. Recent studies on c-MYC have identified it as a key factor in tumor metabolism immunity and a major regulator of metabolic reprogramming, stimulating glycolysis, nucleotide metabolism, and glutamine metabolism [51, 73].Although some studies have indicated that silencing CXCR4 in T-cell acute lymphoblastic leukemia can inhibit the expression of myc [74]. However, we first demonstrated the transcriptional regulation of Pfkfb3 by MYC in macrophages. But in the process of knocking down CXCR4, only Pfkfb3 among the key enzymes of glucose metabolism decreased. As the gene identified as the first in macrophages, the exact reason behind this difference is not yet clear, but it suggests that Pfkfb3 plays a critical role in metabolism during macrophage M1 polarization.

Fibrosis issues associated with chronic prostatitis have gradually been noticed. [2, 4, 6, 7]. It is worth noting that there is a certain association between the infiltration of inflammatory cells (such as macrophages) and prostatic fibrosis. However, it remains to be verified whether the effects produced by activated macrophages are necessary for the occurrence and development of prostatic fibrosis. Based on this, the experimental data demonstrate that reducing CXCR4 expression in EAP mice significantly

reduces the degree of inflammation infiltration and fibrosis. Co-culture studies in vitro also confirmed that silencing CXCR4 in macrophages reduces their role in promoting proliferation and activation of stromal fibroblasts. These results clearly indicate the important role of CXCR4 in promoting macrophages in prostatic fibrosis.

Excessive smooth muscle contraction may contribute to the development of lower urinary tract symptoms (LUTS) in men, either as a primary factor or in conjunction with other pathological processes [75, 76]. Given the critical role of abnormal smooth muscle contraction in the development of LUTS, drugs that target smooth muscle contraction, such as 5α-reductase inhibitors and α1-adrenergic receptor antagonists, are commonly used in clinical practice [77]. ECM deposition and fibrosis are prominent characteristics of periurethral prostate tissue in men with LUTS [21]. The prostatic stroma is primarily composed of smooth muscle cells along with their associated connective tissue, blood vessels, and nerves [78]. Relaxation of smooth muscle cells may disrupt the mechanical dynamics of the extracellular matrix components in the prostatic stroma, potentially promoting fibrosis through the TGF-β1 signaling pathway [79]. Therefore, understanding the molecular mechanisms that link abnormal contraction of smooth muscle cells around the prostate with prostate fibrosis could enhance the treatment response for chronic pelvic pain syndrome (CP/CPPS).In conclusion, we show here that CXCR4, by affecting glucose metabolism, mediates macrophage polarization. Blocking the expression of CXCR4 can inhibit the activation of fibroblasts, improve the fibrotic lesions of chronic prostatitis. Although this experiment still has limitations and further research is needed, we have demonstrated the important role of metabolic reprogramming of macrophage polarization in the state of fibroblasts. These studies also provide new perspectives on the close relationship between chronic prostatitis and prostatic fibrosis, as well as new targets for clinical treatment.

Supplementary Information

The online version contains supplementary material available at https://doi.org/10.1186/s12964-024-01828-y.

Supplementary Material 1.

Supplementary Material 2.

Supplementary Material 3: Figure S1. Silencing CXCR4 alleviates polarization in BMDM and detection of inflammatory factors in the supernatant. (A) Quantitative analysis of Fig. 1B protein. (B) After silencing CXCR4 to induce M1 polarization in iBMDM and culturing for 24 h, the content of inflammatory factors in the cell culture supernatant was detected. (C) Quantitative analysis of Fig. 1D protein. Silence and overexpression of CXCR4 in bone marrow-derived macrophages for LPS (100 ng/ml, 24 h) induction of polarization. (D) The efficiency of knocking down CXCR4 in macrophages was detected by PCR. (E) WB detection of CXCR4, iNOS, Arg1and Pfkfb3 expression. (F) Glucose uptake experiment. (G) Mitochondrial function detection experiment. ns, Not Significant. ***$p<0.001$, **$p<0.01$, *$p<0.05$.

Supplementary Material 4: Figure S2. Quantitative analysis of relevant proteins and silencing PFKFB3 can alleviate M1 polarization of macrophages. (A) Quantitative analysis of Fig. 3F protein. (B) Quantitative analysis of Fig. 4B protein. (C) Quantitative analysis of Fig. 4C protein. After silencing PFKFB3 in iBMDM macrophages, LPS (100 ng/ml, 24 h) induces M1 polarization. (D) The efficiency of knocking down Pfkfb3 in macrophages was detected by PCR. (E) WB detection of iNOS, Arg1 and Pfkfb3 expression. (F) Glucose uptake experiment. (G) Mitochondrial function detection experiment. ns, Not Significant. ***$p<0.001$, **$p<0.01$, *$p<0.05$.

Supplementary Material 5: Figure S3. Detection of CXCL12 expression in human prostate tissue, quantification of inflammatory cytokines in mouse serum, and related protein analysis. (A) According to the H&E and pathological results, the human prostate hyperplasia tissues are divided into the inflammation group and the non-inflammation group, and the WB detects the protein content of CXCL12. (B)Quantitative analysis of Fig. 6 D protein. (C) The ELISA assay detected changes in the levels of inflammatory factors, including IL1β, IL6, and TNF-α, in the serum of four groups of mice: Control, EAP, EAP + Sh NC, and EAP + Sh CXCR4. (D) Quantitative analysis of Fig. 6I protein. ns, Not Significant. ***$p<0.001$, **$p<0.01$, *$p<0.05$.

Supplementary Material 6: Figure S4. Quantitative analysis of related proteins and inhibition of Pfkfb3 help alleviate the degree of prostatic fibrosis in EAP.(A) Quantitative analysis of Fig. 7E protein. (B) Quantitative analysis of Fig. 7I protein. We injected 3PO (PFKFB3 inhibitor, 30 mg/kg/d, every other day, for three consecutive weeks) or vehicle into the peritoneal cavity of EAP mice. (C) Masson staining and IHC were used to detect the degree of fibrosis in EAP mouse prostate tissues. (D) mRNA levels of α-SMA, Col1a1, and Timp1 were examined in mouse prostate tissues. (E) Protein levels of α-SMA, Collagen I, and Timp1 were detected in mouse prostate tissues. ns, Not Significant. ***$p<0.001$, **$p<0.01$, *$p<0.05$.

Supplementary Material 7: Figure S5. (A) Quantitative analysis of Fig. 8C protein. (B) Quantitative analysis of Fig. 8D protein. ns, Not Significant. ***$p<0.001$, **$p<0.01$, *$p<0.05$.

Acknowledgements
We sincerely thank the team of Academician Shao Feng for the gift of iBMDM cells. We wish to thank the Center for Scientific Research of the First Affiliated Hospital of Anhui Medical University for valuable help in seahorse experiments. Thanks for Dr. Dandan Zang's guidance and assistance with the seahorse experiment.

Conflicts of interest disclosure
None.

Authors' contributions
LZ, XC and CJ: conception and design this study; ZY, FR and ZC: collection and assembly of data; PW, SJ, XWL, MWM, ZY, FR and ZC: data Analysis and interpretation; ZY: manuscript writing. Final Approval of Manuscript: All the authors.

Funding
The National Natural Science Foundation of China 82170787, 82300872, and 82370776.

Availability of data and materials
No datasets were generated or analysed during the current study.

Declarations

Competing interests
The authors declare no competing interests.

Received: 17 June 2024 Accepted: 14 September 2024
Published online: 26 September 2024

References

1. Krieger JN, Riley DE, Cheah PY, Liong ML, Yuen KH. Epidemiology of prostatitis: new evidence for a world-wide problem. World J Urol. 2003;21(2):70–4.
2. Blaivas JG. Obstructive uropathy in the male. Urol Clin North Am. 1996;23(3):373–84.
3. Rodriguez-Nieves JA, Macoska JA. Prostatic fibrosis, lower urinary tract symptoms, and BPH. Nat Rev Urol. 2013;10(9):546–50.
4. Robert G, Descazeaud A, Nicolaiew N, Terry S, Sirab N, Vacherot F, Maille P, Allory Y, de la Taille A. Inflammation in benign prostatic hyperplasia: a 282 patients' immunohistochemical analysis. Prostate. 2009;69(16):1774–80.
5. Huang XH, Qin B, Liang YW, Wu QG, Li CZ, Wei GS, Ji HC, Liang YB, Chen HQ, Guan T. LUTS in BPH patients with histological prostatitis before and after transurethral resection of the prostate. Zhonghua Nan Ke Xue. 2013;19(1):35–9.
6. St Sauver JL, Jacobson DJ, McGree ME, Girman CJ, Lieber MM, Jacobsen SJ: Longitudinal association between prostatitis and development of benign prostatic hyperplasia. Urology. 2008;71(3):475–479; discussion 479.
7. Krieger JN, Lee SW, Jeon J, Cheah PY, Liong ML, Riley DE. Epidemiology of prostatitis. Int J Antimicrob Agents. 2008;31 Suppl 1(Suppl 1):S85-90.
8. Bushman WA, Jerde TJ. The role of prostate inflammation and fibrosis in lower urinary tract symptoms. Am J Physiol Renal Physiol. 2016;311(4):F817–21.
9. Wynn TA. Cellular and molecular mechanisms of fibrosis. J Pathol. 2008;214(2):199–210.
10. Hinz B. Formation and function of the myofibroblast during tissue repair. J Invest Dermatol. 2007;127(3):526–37.
11. Pohlers D, Brenmoehl J, Loffler I, Muller CK, Leipner C, Schultze-Mosgau S, Stallmach A, Kinne RW, Wolf G. TGF-beta and fibrosis in different organs - molecular pathway imprints. Biochim Biophys Acta. 2009;1792(8):746–56.
12. Theyer G, Kramer G, Assmann I, Sherwood E, Preinfalk W, Marberger M, Zechner O, Steiner GE. Phenotypic characterization of infiltrating leukocytes in benign prostatic hyperplasia. Lab Invest. 1992;66(1):96–107.
13. Zhang ZY, Zug C, Schluesener HJ. Sphingosine 1-phosphate receptor modulator FTY720 suppresses rat experimental autoimmune prostatitis. Scand J Immunol. 2011;73(6):546–53.
14. Weidenbusch M, Anders HJ. Tissue microenvironments define and get reinforced by macrophage phenotypes in homeostasis or during inflammation, repair and fibrosis. J Innate Immun. 2012;4(5–6):463–77.
15. Perciani CT, MacParland SA. Lifting the veil on macrophage diversity in tissue regeneration and fibrosis. Sci Immunol. 2019;4(40):eaaz0749.
16. Cao Q, Wang Y, Harris DC. Macrophage heterogeneity, phenotypes, and roles in renal fibrosis. Kidney Int Suppl (2011). 2014;4(1):16–9.
17. Tacke F, Zimmermann HW. Macrophage heterogeneity in liver injury and fibrosis. J Hepatol. 2014;60(5):1090–6.
18. Bruscia EM, Bonfield TL. Cystic Fibrosis Lung Immunity: The Role of the Macrophage. J Innate Immun. 2016;8(6):550–63.
19. Buechler MB, Fu W, Turley SJ. Fibroblast-macrophage reciprocal interactions in health, fibrosis, and cancer. Immunity. 2021;54(5):903–15.
20. Lu L, Li J, Jiang X, Bai R. CXCR4/CXCL12 axis: "old" pathway as "novel" target for anti-inflammatory drug discovery. Med Res Rev. 2024;44(3):1189–220.
21. Gharaee-Kermani M, Kasina S, Moore BB, Thomas D, Mehra R, Macoska JA. CXC-type chemokines promote myofibroblast phenoconversion and prostatic fibrosis. PLoS ONE. 2012;7(11):e49278.
22. Rodriguez-Nieves JA, Patalano SC, Almanza D, Gharaee-Kermani M, Macoska JA. CXCL12/CXCR4 Axis Activation Mediates Prostate Myofibroblast Phenoconversion through Non-Canonical EGFR/MEK/ERK Signaling. PLoS ONE. 2016;11(7):e0159490.
23. Van Schaftingen E, Lederer B, Bartrons R, Hers HG. A kinetic study of pyrophosphate: fructose-6-phosphate phosphotransferase from potato tubers. Application to a microassay of fructose 2,6-bisphosphate. Eur J Biochem. 1982;129(1):191–5.
24. De Bock K, Georgiadou M, Schoors S, Kuchnio A, Wong BW, Cantelmo AR, Quaegebeur A, Ghesquiere B, Cauwenberghs S, Eelen G, et al. Role of PFKFB3-driven glycolysis in vessel sprouting. Cell. 2013;154(3):651–63.
25. Wong D, Korz W. Translating an Antagonist of Chemokine Receptor CXCR4: from bench to bedside. Clin Cancer Res. 2008;14(24):7975–80.
26. Acosta-Martinez M, Cabail MZ. The PI3K/Akt Pathway in Meta-Inflammation. Int J Mol Sci. 2022;23(23):15330.
27. Todosenko N, Yurova K, Vulf M, Khaziakhmatova O, Litvinova L. Prohibitions in the meta-inflammatory response: a review. Front Mol Biosci. 2024;11:1322687.
28. Zhang F, Meng T, Feng R, Jin C, Zhang S, Meng J, Zhang M, Liang C. MIF aggravates experimental autoimmune prostatitis through activation of the NLRP3 inflammasome via the PI3K/AKT pathway. Int Immunopharmacol. 2024;141:112891.
29. Sun D, Xing D, Wang D, Liu Y, Cai B, Deng W, Hu Q, Ma W, Jin B. The Protective Effects of Bushen Daozhuo Granule on Chronic Non-bacterial Prostatitis. Front Pharmacol. 2023;14:1281002.
30. Feng JL, Hou D, Zhao C, Bao BH, Huang SY, Deng S, Meng FC, Zhao Q, Wang B, Li HS, et al. A rat study model of depression-driven chronic prostatitis by modulating the PI3K/Akt/mTOR network. Andrologia. 2022;54(8):e14488.
31. True LD, Berger RE, Rothman I, Ross SO, Krieger JN. Prostate histopathology and the chronic prostatitis/chronic pelvic pain syndrome: a prospective biopsy study. J Urol. 1999;162(6):2014–8.
32. John H, Barghorn A, Funke G, Sulser T, Hailemariam S, Hauri D, Joller-Jemelka H. Noninflammatory chronic pelvic pain syndrome: immunological study in blood, ejaculate and prostate tissue. Eur Urol. 2001;39(1):72–8.
33. Liu Y, Li Y, Liu Q, Wu Z, Cui J, Zhu K, Zhao H, Zhou C, Shi B. Role of GM-CSF in a mouse model of experimental autoimmune prostatitis. Am J Physiol Renal Physiol. 2019;317(7):F23–9.
34. Bosco MC. Macrophage polarization: Reaching across the aisle? J Allergy Clin Immunol. 2019;143(4):1348–50.
35. Rao J, Wang H, Ni M, Wang Z, Wang Z, Wei S, Liu M, Wang P, Qiu J, Zhang L, et al. FSTL1 promotes liver fibrosis by reprogramming macrophage function through modulating the intracellular function of PKM2. Gut. 2022;71(12):2539–50.
36. Wu L, Lin H, Li S, Huang Y, Sun Y, Shu S, Luo T, Liang T, Lai W, Rao J, et al. Macrophage iron dyshomeostasis promotes aging-related renal fibrosis. Aging Cell. 2024:e14275.
37. Motrich RD, Breser ML, Sanchez LR, Godoy GJ, Prinz I, Rivero VE. IL-17 is not essential for inflammation and chronic pelvic pain development in an experimental model of chronic prostatitis/chronic pelvic pain syndrome. Pain. 2016;157(3):585–97.
38. Hua X, Ge S, Zhang M, Mo F, Zhang L, Zhang J, Yang C, Tai S, Chen X, Zhang L, et al. Pathogenic Roles of CXCL10 in Experimental Autoimmune Prostatitis by Modulating Macrophage Chemotaxis and Cytokine Secretion. Front Immunol. 2021;12:706027.
39. Chen J, Meng J, Li X, Li X, Liu Y, Jin C, Zhang L, Hao Z, Chen X, Zhang M, et al. HA/CD44 Regulates the T Helper 1 Cells Differentiation by Activating Annexin A1/Akt/mTOR Signaling to Drive the Pathogenesis of EAP. Front Immunol. 2022;13:875412.
40. Li M, Yang Y, Xiong L, Jiang P, Wang J, Li C. Metabolism, metabolites, and macrophages in cancer. J Hematol Oncol. 2023;16(1):80.
41. Sies H, Jones DP. Reactive oxygen species (ROS) as pleiotropic physiological signalling agents. Nat Rev Mol Cell Biol. 2020;21(7):363–83.
42. Schieber M, Chandel NS. ROS function in redox signaling and oxidative stress. Curr Biol. 2014;24(10):R453-462.
43. Holmstrom KM, Finkel T. Cellular mechanisms and physiological consequences of redox-dependent signalling. Nat Rev Mol Cell Biol. 2014;15(6):411–21.
44. Tran N, Mills EL. Redox regulation of macrophages Redox Biol. 2024;72:103123.
45. LeFort KR, Rungratanawanich W, Song BJ. Contributing roles of mitochondrial dysfunction and hepatocyte apoptosis in liver diseases through oxidative stress, post-translational modifications, inflammation, and intestinal barrier dysfunction. Cell Mol Life Sci. 2024;81(1):34.
46. Green DR. The Mitochondrial Pathway of Apoptosis Part II: The BCL-2 Protein Family. Cold Spring Harb Perspect Biol. 2022;14(6):a041046.
47. Mouton AJ, Li X, Hall ME, Hall JE. Obesity, Hypertension, and Cardiac Dysfunction: Novel Roles of Immunometabolism in Macrophage Activation and Inflammation. Circ Res. 2020;126(6):789–806.
48. Saha S, Shalova IN, Biswas SK. Metabolic regulation of macrophage phenotype and function. Immunol Rev. 2017;280(1):102–11.
49. Van Schaftingen E, Jett MF, Hue L, Hers HG. Control of liver 6-phosphofructokinase by fructose 2,6-bisphosphate and other effectors. Proc Natl Acad Sci U S A. 1981;78(6):3483–6.

50. Ni X, Lu CP, Xu GQ, Ma JJ. Transcriptional regulation and post-translational modifications in the glycolytic pathway for targeted cancer therapy. Acta Pharmacol Sin. 2024;45(8):1533–55.
51. Venkatraman S, Balasubramanian B, Thuwajit C, Meller J, Tohtong R, Chutipongtanate S. Targeting MYC at the intersection between cancer metabolism and oncoimmunology. Front Immunol. 2024;15:1324045.
52. D'Souza LC, Shekher A, Challagundla KB, Sharma A, Gupta SC. Reprogramming of glycolysis by chemical carcinogens during tumor development. Semin Cancer Biol. 2022;87:127–36.
53. Linton MF, Moslehi JJ, Babaev VR. Akt Signaling in Macrophage Polarization, Survival, and Atherosclerosis. Int J Mol Sci. 2019;20(11):2703.
54. Covarrubias AJ, Aksoylar HI, Horng T. Control of macrophage metabolism and activation by mTOR and Akt signaling. Semin Immunol. 2015;27(4):286–96.
55. Vergadi E, Ieronymaki E, Lyroni K, Vaporidi K, Tsatsanis C. Akt Signaling Pathway in Macrophage Activation and M1/M2 Polarization. J Immunol. 2017;198(3):1006–14.
56. Yang H, Cheng H, Dai R, Shang L, Zhang X, Wen H. Macrophage polarization in tissue fibrosis. PeerJ. 2023;11:e16092.
57. Wen JH, Li DY, Liang S, Yang C, Tang JX, Liu HF. Macrophage autophagy in macrophage polarization, chronic inflammation and organ fibrosis. Front Immunol. 2022;13:946832.
58. Zhang M, Liu Y, Chen J, Chen L, Zhang L, Chen X, Hao Z, Liang C. Targeting CXCL12/CXCR4 Signaling with AMD3100 Might Selectively Suppress CXCR4+ T-Cell Chemotaxis Leading to the Alleviation of Chronic Prostatitis. J Inflamm Res. 2022;15:2551–66.
59. Loetscher M, Geiser T, O'Reilly T, Zwahlen R, Baggiolini M, Moser B. Cloning of a human seven-transmembrane domain receptor, LESTR, that is highly expressed in leukocytes. J Biol Chem. 1994;269(1):232–7.
60. Li F, Peng J, Lu Y, Zhou M, Liang J, Le C, Ding J, Wang J, Dai J, Wan C, et al. Blockade of CXCR4 promotes macrophage autophagy through the PI3K/AKT/mTOR pathway to alleviate coronary heart disease. Int J Cardiol. 2023;392:131303.
61. Ma Q, Zhang N, You Y, Zhu J, Yu Z, Chen H, Xie X, Yu H. CXCR4 blockade in macrophage promotes angiogenesis in ischemic hindlimb by modulating autophagy. J Mol Cell Cardiol. 2022;169:57–70.
62. Tang C, Lei X, Xiong L, Hu Z, Tang B. HMGA1B/2 transcriptionally activated-POU1F1 facilitates gastric carcinoma metastasis via CXCL12/CXCR4 axis-mediated macrophage polarization. Cell Death Dis. 2021;12(5):422.
63. Hua X, Zhang J, Ge S, Liu H, Du H, Niu Q, Chen X, Yang C, Zhang L, Liang C. CXCR3 antagonist AMG487 ameliorates experimental autoimmune prostatitis by diminishing Th1 cell differentiation and inhibiting macrophage M1 phenotypic activation. Prostate. 2022;82(13):1223–36.
64. Okoye CN, Koren SA, Wojtovich AP. Mitochondrial complex I ROS production and redox signaling in hypoxia. Redox Biol. 2023;67:102926.
65. Wang H, Gao L, Zhao C, Fang F, Liu J, Wang Z, Zhong Y, Wang X. The role of PI3K/Akt signaling pathway in chronic kidney disease. Int Urol Nephrol. 2024;56(8):2623–33.
66. Liu Y, Kong H, Cai H, Chen G, Chen H, Ruan W. Progression of the PI3K/Akt signaling pathway in chronic obstructive pulmonary disease. Front Pharmacol. 2023;14:1238782.
67. Joo K, Karsulovic C, Sore M, Hojman L. Pivotal Role of mTOR in Non-Skin Manifestations of Psoriasis. Int J Mol Sci. 2024;25(12):6778.
68. Guo Y, Wang P, Hu B, Wang L, Zhang Y, Wang J. Kongensin A targeting PI3K attenuates inflammation-induced osteoarthritis by modulating macrophage polarization and alleviating inflammatory signaling. Int Immunopharmacol. 2024;142(Pt A):112948.
69. Lin J, Lin HW, Wang YX, Fang Y, Jiang HM, Li T, Huang J, Zhang HD, Chen DZ, Chen YP. FGF4 ameliorates the liver inflammation by reducing M1 macrophage polarization in experimental autoimmune hepatitis. J Transl Med. 2024;22(1):717.
70. Zhang Y, Yan C, Dong Y, Zhao J, Yang X, Deng Y, Su L, Yin J, Zhang Y, Sun F, et al. ANGPTL3 accelerates atherosclerotic progression via direct regulation of M1 macrophage activation in plaque. J Adv Res. 2024.
71. Dussold C, Zilinger K, Turunen J, Heimberger AB, Miska J. Modulation of macrophage metabolism as an emerging immunotherapy strategy for cancer. J Clin Invest. 2024;134(2):e175445.
72. Shi L, Pan H, Liu Z, Xie J, Han W. Roles of PFKFB3 in cancer. Signal Transduct Target Ther. 2017;2:17044.
73. Purhonen J, Klefstrom J, Kallijarvi J. MYC-an emerging player in mitochondrial diseases. Front Cell Dev Biol. 2023;11:1257651.
74. Ma W, Wan Y, Zhang J, Yao J, Wang Y, Lu J, Liu H, Huang X, Zhang X, Zhou H, et al. Growth arrest-specific protein 2 (GAS2) interacts with CXCR4 to promote T-cell leukemogenesis partially via c-MYC. Mol Oncol. 2022;16(20):3720–34.
75. Macoska JA, Uchtmann KS, Leverson GE, McVary KT, Ricke WA. Prostate Transition Zone Fibrosis is Associated with Clinical Progression in the MTOPS Study. J Urol. 2019;202(6):1240–7.
76. Roman K, Murphy SF, Done JD, McKenna KE, Schaeffer AJ, Thumbikat P. Role of PAR2 in the Development of Lower Urinary Tract Dysfunction. J Urol. 2016;196(2):588–98.
77. Ma J, Gharaee-Kermani M, Kunju L, Hollingsworth JM, Adler J, Arruda EM, Macoska JA. Prostatic fibrosis is associated with lower urinary tract symptoms. J Urol. 2012;188(4):1375–81.77.
78. Chagas MA, Babinski MA, Costa WS, Sampaio FJ. Stromal and acinar components of the transition zone in normal and hyperplastic human prostate. BJU Int. 2002;89(7):699–702.
79. Delella FK, Lacorte LM, Almeida FL, Pai MD, Felisbino SL. Fibrosis-related gene expression in the prostate is modulated by doxazosin treatment. Life Sci. 2012;91(25–26):1281–7.

Publisher's Note